

**Pathophysiological Cardiac Remodeling And
The Potential Of Cellular And Molecular Therapy**

BY

SHWETHA MURELI
B.Tech., SASTRA University, 2010

THESIS

Submitted as partial fulfillment of the requirements
for the degree of Master of Science in Bioengineering
in the Graduate College of the
University of Illinois at Chicago, 2013

Chicago, Illinois

Defense Committee:

Dr. Kathrin Banach, Advisor, Department of Medicine (Section of Cardiology)
Dr. Brenda Russell, Department of Physiology and Biophysics
Dr. Thomas J Royston

ACKNOWLEDGMENTS

I would like to thank my thesis advisor Dr. Kathrin Banach who provided guidance in all areas that helped me accomplish my research goals and enjoy myself in the process. I would like to thank my committee members, Dr. Brenda Russell and Dr. Thomas J Royston for their participation and support. I would also like to acknowledge Dr. Dan J Bare, who helped me achieve several goals in the project and also made contributions important to the conduct of the study and Dr. Jaime DeSantiago for his constant guidance and invaluable suggestions in studies pertaining to electrophysiology.

I would also like to thank my family members (parents and sister) and friends (Kartik, Rajni, Dharini, Lakshmi, Vasanth, Raghuram) who had been there through this time and ensured that I stayed on track to finish this work successfully.

TABLE OF CONTENTS

<u>CHAPTER 1</u>	<u>PAGE</u>
1. INTRODUCTION.....	1
1.1 Cardiac remodeling.....	1
1.2 Cardiac physiological properties.....	3
1.3 Rational for the study.....	8
2. MATERIALS AND METHODS.....	11
2.1 Cell culture.....	11
2.1.1 Mesenchymal stem cell culture.....	11
2.1.2 <i>HL-1</i> cell culture.....	11
2.2 Multi-electrode arrays.....	12
2.2.1 Theory.....	12
2.2.2 Multi-electrode array recordings.....	14
2.2.3 Electrophysiological recordings evaluating conditioned media/tyrode.....	16
2.3 Conditioned medium/tyrode preparation.....	17
2.4 Co-culture and dye diffusion assay.....	17
2.5 Quantitative reverse transcriptase polymerase chain reaction.....	18
2.6 Pharmacological treatment of <i>HL-1</i> cells.....	19
2.7 Sodium dodecyl sulfate polyacrylamide gel electrophoresis and western blotting.....	20
2.8 Statistical analysis.....	21
3. RESULTS.....	22
3.1 Mesenchymal stem cells modulate the spontaneous activity of <i>HL-1</i> cells.....	22
3.2 <i>HL-1</i> cells and mesenchymal stem cells establish intercellular coupling via gap junctions.....	23
3.3 Conditioned tyrode mediated upregulation of connexin43 depends on β -catenin and glycogen synthase kinase 3- β	30
4. DISCUSSION.....	37
4.1 Influence of non-excitable cells on cardiac excitation spread.....	37
4.2 Influence of mesenchymal stem cells on <i>HL-1</i> cell excitability and beating frequency.....	39
4.3 Mesenchymal stem cells mediated upregulation of connexin 43.....	39
4.4 Mesenchymal stem cells mediated paracrine signaling.....	40
5. CONCLUSION.....	43

TABLE OF CONTENTS (continued)

<u>CHAPTER 2</u>	<u>PAGE</u>
1. INTRODUCTION.....	44
1.1 Transverse-tubule network.....	44
1.2 Transverse-tubule regulation and remodeling.....	46
2. MATERIALS AND METHODS.....	49
2.1 Cell isolation and culture.....	49
2.2 Pharmacological treatment of rabbit ventricular myocytes.....	50
2.3 Field stimulation of rabbit ventricular myocytes.....	50
2.4 Transverse-tubule imaging.....	51
2.5 Image analysis.....	51
2.6 Statistical analysis.....	53
3. RESULTS.....	54
3.1 Inhibition of nicotinamide adenine dinucleotide phosphate-oxidase-dependent reactive oxygen species production modulates transverse-tubule network.....	54
3.2 Effect of mitochondrial and cytoplasmic reactive oxygen species and transverse-tubule remodeling.....	60
4. DISCUSSION.....	62
5. CONCLUSION.....	65
6. FUTURE DIRECTIONS.....	65
REFERENCES.....	66
VITA.....	81

LIST OF FIGURES

<u>FIGURES</u>	<u>PAGE</u>
1. Schematic cardiac action potential.....	4
2. Schematic drawing of gap junction channels.....	6
3. A pictorial representation of the electrical coupling between a cell and a planar electrode.....	13
4. Field potential recordings using multi-electrode arrays.....	15
5. Mesenchymal stem cells modify the electrophysiological properties of cardiomyocytes.....	23
6. Mesenchymal stem cells establish intercellular coupling with cardiomyocytes.....	24
7. Paracrine factors secreted by MSCs increase the conduction velocity of <i>HL-1</i> monolayers.....	26
8. MSC-conditioned medium increases connexin43 expression in cardiomyocytes.....	28
9. β -catenine inhibition prevents the ConT-mediated increase in Cx43 protein levels...	29
10. Lithium inhibition of GSK 3- β mimics the effect of ConT on θ and Cx43 protein expression.....	31
11. ConM-mediated increase in θ does not depend on PI3K/Akt signaling.....	32
12. ConT-mediated changes depend upon the activation of LRP6 through agonists of the canonical Wnt-signaling pathway.....	34
13. Canonical Wnt signaling and ERK 1/2 signaling pathways affect Cx43 expression.....	36
14. Schematic summary of the experimental results illustrates the proposed transduction pathway.....	43

LIST OF FIGURES (continued)

<u>FIGURES</u>	<u>PAGE</u>
15. Schematic representation of the t-tubular system and the neighboring protein machinery.....	45
16. Schematic representation of the major steps involved in image analysis by fast fourier transform (FFT) technique.....	52
17. Confocal image of di-8-ANEPPS stained t-tubules and the corresponding power spectrum depicting t-tubular density.....	55
18. Inhibition of NOX dependent ROS production modulates the rate of t-tubular loss.....	57
19. Integrity of t-tubular system in paced and non-paced conditions.....	59
20. Inhibition of cytoplasmic and mitochondrial-ROS production does not reduce the rate of t-tubule loss in non-paced VMs.....	61

LIST OF ABBREVIATIONS

Akt	Protein Kinase B
AMI	Acute Myocardial Infarction
AP	Action Potential
ATP	Adenosine Triphosphate
AV	Atrioventricular
BIN1	Myc Box-Dependent-Interacting Protein 1
BMSC	Bone Marrow Derived Stem Cell
cDNA	Copy Deoxyribosenucleic Acid
CICR	Calcium-Induced Calcium Release
ConM	Conditioned Medium
ConT	Conditioned Tyrode
Ctrl	Control
Cx	Connexin
DMEM	Dulbecco's Modified Eagle Medium
DNA	Deoxyribosenucleic Acid
EAD	Early After Depolarization
ECC	Excitation-Contraction Coupling
EDTA	Ethylenediaminetetraacetic acid
ERK	Extracellular Signal-Regulated Kinase
ESC	Embryonic Stem Cell
FBS	Fetal Bovine Serum
FFT	Fast Fourier Transform
GAPDH	Glyceraldehyde 3-Phosphate Dehydrogenase
GSK	Glycogen Synthase Kinase

LIST OF ABBREVIATIONS (continued)

HF	Heart Failure
IGF-1	Insulin Growth Factor-1
iPSC	Induced Pluripotent Stem Cell
IWP	Inhibitor of Wnt Production
kHz	Kilo Hertz
KO	Knockout
LiCl	Lithium Chloride
LRP6	Lipoprotein Receptor Protein-6
LV	Left Ventricular
LVH	Left Ventricular Hypertrophy
MAPK	Mitogen-Activated Protein Kinase
MEA	Multi-Electrode Array
MMP	Matrix Metalloproteinases
mRNA	Messenger Ribonucleic Acid
MSC	Mesenchymal Stem Cell
NADPH	Nicotinamide-Adenine Dinucleotide Phosphate
NCX	Sodium Calcium Exchanger
NKA	Sodium Potassium ATPase
NOS	Nitrous Oxide Synthase
NOX	NADPH Oxidase
<i>p</i>	Phospho
PBS	Phosphate Buffered Saline
PI3K	Phosphoinositide 3-Kinase
qPCR	Quantitate Polymerase Chain Reaction

LIST OF ABBREVIATIONS (continued)

RNA	Ribonucleic acid
ROS	Reactive Oxygen Species
rpm	Rotation Per Minute
RT-PCR	Reverse Transcriptase Polymerase Chain Reaction
RTK	Receptor Tyrosine Kinase
RyR	Ryanodine Receptor
SA	Sinoatrial
SDS-PAGE	Sodium Dodecyl Sulfate-Polyacrylamide Gel Electrophoresis
SEM	Standard Error of Mean
SERCA	Sarcoplasmic Reticulum Ca ²⁺ ATPase
sFRP	Secreted Frizzled-Related Protein
SR	Sarcoplasmic Reticulum
VEGF	Vascular Endothelial Growth Factor
VEGF R2	Vascular Endothelial Growth Factor Receptor 2
VM	Ventricular Myocyte
XO	Xanthine Oxidase
μm	Micrometer
β-ME	β-Mercaptoethanol

SUMMARY

CHAPTER 1

Ischemic heart disease leads to a sudden death of cardiomyocytes and loss of normal cardiac function due to an ischemic insult to the myocardium. Regenerative therapeutic strategies such as stem cell transplantation are being widely used to regenerate or repair the infarcted myocardium and restore normal cardiac function. Mesenchymal stem cells (MSCs) are known to alleviate arrhythmias and improve conduction when transplanted into cardiac tissue; however, the mechanism was not yet determined. Therefore, this study was aimed to determine the mechanism by which MSCs modulate the excitability and conduction in cardiac tissue after transplantation by testing the hypothesis that MSCs modulate conduction i. by intercellular coupling with cardiomyocytes or ii. by paracrine signaling.

Cardiomyocyte monolayers derived from *HL-1* cells were plated on microelectrode arrays (MEAs) and their spontaneous activity and conduction velocity (θ) was determined from field potential recordings. When *HL-1* monolayers were co-cultured with MSCs, the beating frequency was significantly attenuated over time with no significant change in θ . However, when monolayers were incubated with MSC conditioned media (ConM), or conditioned tyrode (ConT) θ increased over time without a significant change in beating frequency. Also during the same time frame, expression of the cardiac gap junction isoform connexin (Cx) 43 was upregulated both on the mRNA and protein levels. Cx43 upregulation depended on glycogen synthase kinase-3 (GSK3)/beta-catenin (β -catenin) which was activated in part through MSC-dependent Wnt secretion. Phosphorylation of lipoprotein receptor protein 6 (LRP6), a component of the Wnt receptor complex was attenuated when Wnt secretion from MSCs was suppressed also preventing the increase in θ . Inhibition of β -catenin a downstream target of the canonical Wnt pathway suppressed changes in θ while inhibition of GSK3- α/β and stimulation

SUMMARY (continued)

with exogenous Wnt3 mimicked the effect of ConT. However, in addition an extracellular signal-regulated kinase (ERK) dependent phosphorylation of LRP6 was determined. Inhibition of ERK1/2 resulted in a significant decrease in ConT-mediated change in θ . Overall the study indicates that while MSCs establish intercellular coupling with cardiomyocytes and can suppress their excitability, they can influence cardiac conduction through paracrine signaling alone.

CHAPTER 2

The transverse-tubule (t-tubule) network ensures the instantaneous and synchronous release of Ca^{2+} throughout the ventricular myocyte. Transverse-tubule (t-tubule) remodeling occurs during pathological conditions and the mechanisms underlying this remodeling are still unclear. This study was aimed to elucidate a mechanism by which t-tubule remodeling occurs. Rabbit ventricular myocytes were cultured for two days and the t-tubule density was determined by di-8-ANEPPS staining at periodic intervals. Inhibition of NADPH oxidase 2-mediated reactive oxygen species (ROS) generation attenuated the rate of t-tubule loss. However, scavenging whole-cell and mitochondrial generated ROS did not decrease the loss of t-tubules over time. These preliminary data suggest that there exists a putative role of ROS in t-tubular remodeling and further studies need to be carried out to investigate the molecular targets that could possibly reverse or attenuate this remodeling.

CHAPTER 1

1. INTRODUCTION

1.1 Cardiac Remodeling

Cardiovascular diseases account for more than 30% of human mortality globally and in 2011 approximately 7.25 million deaths were attributed to ischemic heart disease [1]. Acute Myocardial Infarction (AMI) is one of the predominant pathological conditions that trigger cardiac remodeling which then leads to heart failure (HF). AMI is characterized by a sudden and significant loss of cardiomyocytes due to ischemia in the infarct zone leading to the loss of function of the infarcted myocardium over time. Consequently this results in molecular, cellular and interstitial changes in the infarct tissue which include: hypertrophy of surviving cardiomyocytes, interstitial fibrosis and inflammation, impaired neovascularization and scar formation, dilation and reshaping of left ventricular (LV) wall and finally a reduction in cardiac contractility and output [2, 3]. Clinically, cardiac remodeling is defined as a change in size, shape and function of the heart as a result of changed cardiac load or injury, and can be categorized into either physiological or pathophysiological cardiac remodeling. Physiological cardiac remodeling is a widely observed phenomenon in the hearts of athletes and pregnant women. This type of remodeling involves compensated hypertrophy of the heart with increased LV wall thickness resulting in enhanced cardiac output to meet the high-energy demand of physiological states such as exercise and pregnancy [4]. In pathophysiological cardiac remodeling, the changes that occur at the cellular and molecular level directly translate to maladaptive structural and functional changes in the heart. Compensatory structural remodeling such as the initial ventricular wall-remodeling phase is considered beneficial, as it is associated with maintained or improved cardiac output producing significantly increased LV volumes. Although progressing into HF, this compensatory structural remodeling becomes de-compensatory and is characterized by an increased end-systolic index and decreased ejection

fraction [5]. Also, it has been observed that the infarct size correlates to the magnitude of remodeling change occurring in the myocardium i.e., large infarcts provoke greater dilation and greater increases in systolic and diastolic stress than small infarcts [6]. Therefore it is critical to develop therapeutic strategies that either enhance the regenerative capacity of the cardiac tissue or minimize the damaged area by cell replacement therapy.

Regeneration or repair of an infarcted heart demands the replenishment of the large number of lost cardiomyocytes and their functional integration into the host myocardium. Since the natural regenerative capacity of the heart is very limited (range of 0.45 % - 1% rate of renewal of cardiomyocytes/year) [3], stem cells have been used as a potential source of cellular replacement in tissue in many clinical [7] and pre-clinical studies [8]. Potential sources for stem cells include: embryonic stem cells (ESCs), bone marrow derived stem cells (BMSCs), induced pluripotent stem cells (iPSCs), and mesenchymal stem cells (MSCs) [9, 10]. Strategies of cellular replacement therapy are, the transplantation of i. cardiomyocytes that were differentiated from stem cells *in vitro*, or ii. undifferentiated stem cells. The advantage of the first strategy would be that the cells more easily integrate into the working myocardium and can contribute to cardiac pump function. In the latter case however, stem cells could not only differentiate into cardiomyocytes but also enhance vascularization based on the micro-environmental cues presented to them. It has been demonstrated that both undifferentiated and differentiated stem cells engraft and improve cardiac function after transplantation in studies involving rodent models [11, 12]. Clinical studies using stem cell transplantation predominantly involve bone marrow derived MSCs due to their availability and their demonstrated clinical safety. The *in vivo* and *in vitro* studies demonstrate a beneficial effect of MSC transplantation including reduced infarct size, preserved systolic function and reduced left ventricular remodeling [13-16]; However, a significant portion of the transplanted MSCs disappear from the site of infarct (or site of transplantation) shortly after transplantation [17]. In animal studies,

systemically administered MSCs demonstrated low (2%) engraftment levels and in vitro as well as in vivo exhibited only a limited capacity for transdifferentiation into cardiomyocytes [17]. Thus, one possible mechanism by which MSCs improve cardiac function besides cell differentiation, could be by the reduction in cardiac infarct tissue due to paracrine signaling [18]. In this study we aimed to determine the mechanism by which MSCs can influence cardiomyocyte function after transplantation.

1.2 Cardiac physiological properties

Successful cellular replacement in cardiac tissue depends on how well the transplanted cells functionally integrate into the host myocardium. Functional integration is achieved when the transplanted cells exhibit electromechanical properties similar to the cardiomyocytes and establish intercellular coupling with them [19].

An important indicator of electrical activity in the heart is the cardiac action potential (AP). The AP is the membrane potential waveform that is determined by a complex and tightly regulated interplay of many ion channels and transporters [20]. Figure 2 depicts the predominant ionic currents that modulate the four phases of the cardiac AP.

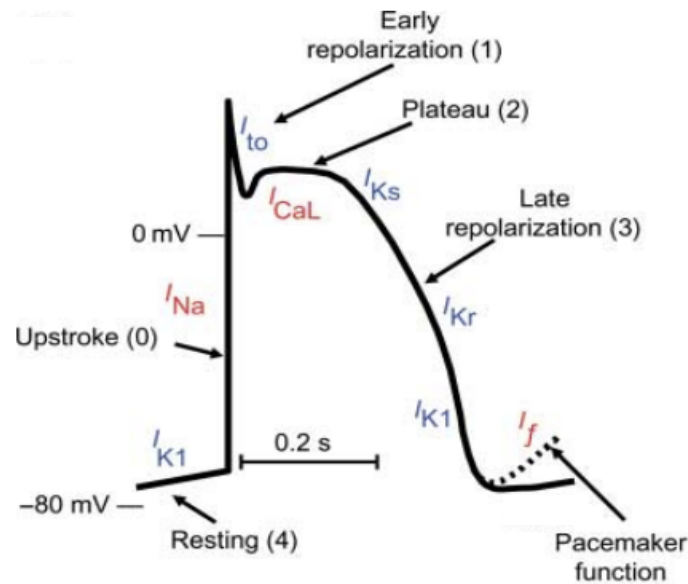


Figure 1: Schematic of the cardiac action potential (AP) indicating the phases of 0: rapid depolarization or AP upstroke; 1: early repolarization; 2: plateau; 3: late repolarization; 4: resting and underlying ionic currents. (Image obtained with permission and modified from [21])

During the resting phase (phase 4) there is an inflow of potassium (K^+) ions into the cell (I_{K1}) due inward-rectifying K^+ channels. This maintains the resting membrane potential of the cell close to the equilibrium potential of K^+ , around -80 mV. Upon electrical stimulation, the rapid activation of voltage sensitive sodium (Na) channels, allows a Na current (I_{Na}) that drives the upstroke of the AP (phase 0). Following this depolarization (phase 0), an early repolarization phase (phase 1) occurs due to out-flow of K^+ ions through a rapidly activating and inactivating transient- outward K^+ channel (I_{to}). Following I_{to} , the cardiomyocytes enter a plateau phase (phase 2) during which the inflow of Ca^{2+} ions ($I_{Ca,L}$) through the L-type Ca^{2+} channels is

balanced by the outward currents (I_{Kr} , I_{Ks}) through the slow activating delayed-rectifier K^+ channels. This time-dependent activation of I_{Kr} and I_{Ks} (phase 3), then enables the cardiomyocyte to come back to its resting phase (phase 4). Additionally, pacemaker cells exhibit gradual depolarization during phase 4, due to a relatively non-selective 'funny' current (I_f).

The Na-dependent up-stroke of the AP forms the driving force of AP propagation by rapidly establishing a voltage gradient between cells that drives further the depolarizing current. The AP duration on the other hand, regulates the refractory period of the cell thereby preventing early re-excitation of the tissue that could lead to arrhythmia. Functional changes in the failing heart can also be attributed to electrical remodeling which alters both cardiac electrophysiology and conduction [22, 23]. Alterations to these phases of the cardiac action potential have been shown to occur in HF where the AP duration is prolonged due to a decrease in I_{Kr} and I_{Ks} [24], K^+ currents (I_{to}) [25] [26] and K^+ currents (I_{K1}) [27] [25] and can result in early after depolarization (EADs). The occurrence of EADs at plateau phase membrane potential can be attributed to reactivation of Ca channels which can partially recover during prolonged AP durations and cause further depolarization [28].

While the AP establishes the excitability of the cardiomyocytes, AP propagation, a prerequisite for the coordinated excitation of the entire cardiac muscle, is guaranteed by gap junction channels. Gap junction channels are formed by a class of transmembrane proteins named connexins (Cx) occurring at the junctions between two adjacent cells. Six connexin protein subunits form a hemichannel termed connexon [29]. The interaction of two connexons located in the cell membranes of adjacent cells allows the functional gap junctions channels to open and allow the exchange of metabolites, ions, second messengers and electrical impulses via passive diffusion between the cytoplasmic compartments of the cells [30]. Figure 1 represents the gap junction channels formed between adjacent cells.

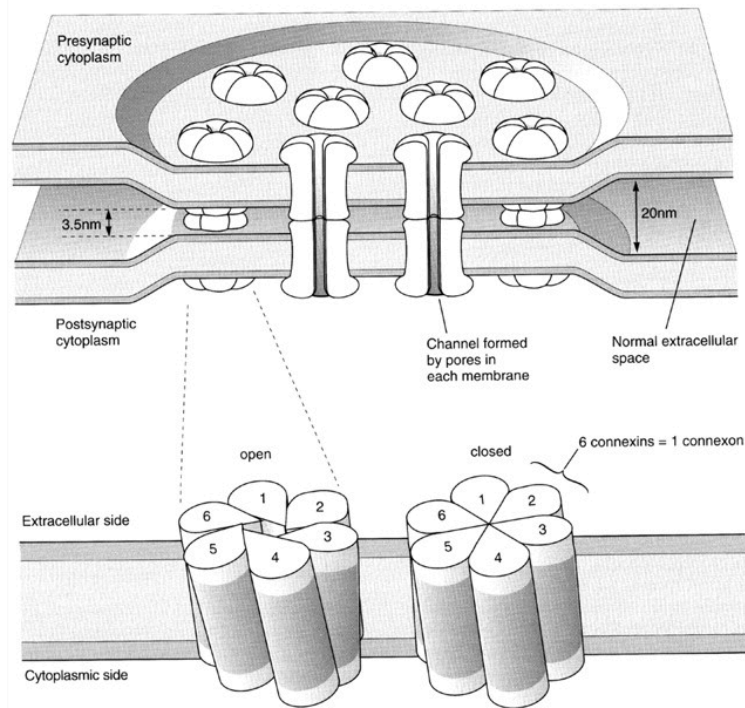


Figure 2: Schematic drawing of gap junction channels. Each apposed cell contributes a hemi-channel to the complete gap junction channel. Each hemi-channel is formed by six protein subunits, called connexins (Cx). Six connexin subunits (connexon) of the hemi-channel may coordinately change configuration to open and close the channel. (Image obtained with permission and modified from [29])

Overall twenty one different connexin isoforms have been identified in humans [29] of which Cx43, Cx40 and Cx45 are the three principal isoforms of connexins found in the cardiac muscle. Cx43 is the predominant isoform expressed in both atrial and ventricular myocardium but absent in the sinoatrial (SA) and atrioventricular (AV) nodes. Cx45 is expressed in the

ventricular conduction system, SA and AV nodes and found in very low levels in the surrounding atria and ventricular myocardium. Cx40 is co-expressed with Cx43 in the atrial myocardium [31, 32] and also co-expressed with Cx45 in the fast-conducting tissues [33]. Due to its low single channel conductance the expression of Cx45 in the atrioventricular node and His bundle may help distinguish the central conductive tissues from the working myocardium. In contrast, Cx40, which has the highest single channel conductance of the 3 cardiac isoforms, allows rapid impulse propagation to distal parts of the conduction system, where Cx43 additionally facilitate coupling to the surrounding working myocytes. This spatially defined expression of connexins provides for the coordinated spread of electrical impulses from the atrial to ventricular chamber [34].

To understand the role of gap junction channels in electrical impulse conduction, the working myocardium can be considered as a three-dimensional network containing of excitable and non-excitable cells. Under physiological conditions, a given cardiomyocyte in the adult working myocardium is electrically coupled to the adjacent cells via gap junctions that are predominantly localized at the intercalated discs [35]. Along with the electrical resistance, the sub-cellular distribution of gap junctions is a critical determinant of the rate of conduction across the myocardium. Unidirectional impulse propagation through the gap junction channels enabled by AP duration and absolute refractory period of the cardiac tissue results in a uniform spread of the excitation wave front from an excited region to a non-excited region of the myocardium. However, under pathophysiological conditions such as decreased pH and increased $[Ca]_i$, gap junction channels between cells close, the total number of channels at the intercalated disc decreases and sub-cellular connexin distribution is altered. These changes lead to increased intercellular resistances, heterogeneous transfer of electrical impulses within the myocardium (heterogeneous excitation wave-front due to varying conduction times) resulting in unidirectional conduction blocks and slowed conduction times [36]. A heterogeneous excitation wave-front

leads to heterogeneous refractoriness and can result in reentry of the excitation into a previously excited area and induce cardiac arrhythmias. Gap junction remodeling like this has been described in HF, where ventricular conduction is slowed with heterogeneous excitation spread due to a reduction in the expression and altered distribution of the Cx43 gap junction protein [23]. Similar findings have also been reported in hypertrophied and ischemic human ventricular myocardium where Cx43 is down regulated and redistributed from the intercalated disk to the cell border (lateralization) leading to slowed conduction [37]. These findings underline that cell integration into the cardiac muscle has to be established by maintaining the intercellular coupling resistance and the non-perturbation of the excitation wave front, which together have to be taken into consideration when transplanting non-excitable cells. *In vitro* studies have demonstrated a reduction in conduction velocity and spontaneous activity when non-excitable cells such as fibroblasts establish intercellular coupling with cardiomyocytes by gap junction coupling. This depending on the cell size and membrane potential can change the myocyte resting membrane potential and increase its capacitive load [38, 39]. Hence, these observations indicate that connexin expression and distribution between excitable as well as non-excitable cells play a critical role in impulse propagation and should be considered as an important factor of efficacy of functional integration of the transplanted cells for cellular replacement and cardiac repair. Therefore, elucidating the mechanisms that regulate connexin expression and distribution is critical to the understanding of both the consequences of cardiac remodeling and the potential mechanisms of cardiac repair.

1.3 Rationale for the study

As discussed above, MSCs are transplanted into cardiac infarct regions as a potential mechanism for cell replacement [40]. When non-excitable cells such as fibroblasts establish intercellular coupling with cardiomyocytes through gap junction channels, they reduce the

spontaneous activity and conduction velocity of the cardiac tissue by increasing the myocytes capacitive load [38, 39]. By bridging the conduction between spatially separated cardiomyocytes [41, 42] they can further increase the heterogeneity of the excitation wave-front and increase the propensity for cardiac arrhythmia [43]. Similarly, MSC transplantation into the myocardium can be pro-arrhythmic [44] and may result from the consequences of intercellular coupling as outlined above. However, it has been demonstrated that the MSCs that remain at the site after transplantation express Cx43 [45] and establish intercellular coupling within the adult myocardium [46-48]. Also, they have been shown to preserve impulse conduction [49], to reduce the inducibility of ventricular arrhythmias [43] and improve atrioventricular conduction (AV) block [50]. However, this preservation of conduction cannot simply be explained by the integration of the MSCs into the tissue therefore, we hypothesized that significant benefit through MSCs is mediated by paracrine signaling. The number of paracrine factors secreted by MSCs is extensive [51] and some of them were shown to facilitate angiogenesis and cardiomyogenesis, to inhibit cardiac remodeling and to stimulate endogenous cardiac progenitor cells [40, 52]. Modifications of the MSC secretome further showed that their cardioprotective effect is sensitive to the composition of signaling molecules secreted [53-56] and the use of conditioned media alone was shown to exhibit a protective effect during ischemia reperfusion injury [14]. Vascular endothelial growth factor (VEGF) [57], IGF-1[58] and secreted frizzled-related protein (sFRP) that is significantly upregulated in the secretome of Akt overexpressing MSCs, have been directly linked to cardiac repair [59, 60]. Decreased infarct size after ischemia reperfusion injury following MSC transplantation may result from either enhanced myocyte survival or through a mechanism of replacement by differentiated MSCs or endogenous stem cells. However, as previously demonstrated, MSC-mediated paracrine signaling significantly influences the calcium handling properties of individual cardiomyocytes and affects their survival [61] thereby changing cellular excitability and contractility. Changes in excitation-contraction

coupling (ECC) can modulate excitation spread and the potential for arrhythmic activity. In addition, components of the MSC secretome like VEGF [62] and Wnt1 [63] have been reported to modulate cardiac gap junction expression [64, 65] further supporting the hypothesis that MSC-mediated paracrine can induce changes in cardiac excitation spread.

Therefore, the aim in the current study was to determine if MSCs mediate changes in cardiac excitability and excitation spread and to identify whether these changes occur through hetero-cellular coupling and/or paracrine signaling.

2. MATERIALS AND METHODS

2.1 Cell culture

2.1.1 MSC culture

Bone marrow derived mesenchymal stem cells (MSCs) was isolated from mouse tibia and femur and were enriched for CD5, CD45R, CD11b, Gr1, TER119 (Murine Progenitor Enrichment Cocktail, Stem-cell Technologies) and found to be Sca-1⁺, CD34⁺, ckit⁺, CD105⁺, CD90.1⁺ positive and negative for CD45⁻ [66, 67]. Mouse bone marrow derived mesenchymal stem cells (MSCs) were cultured and expanded in complete MesenCult® MSC basal medium (mouse) (Stemcell Technologies; Vancouver, Canada) supplemented with penicillin/streptomycin (50 U/ml/ 50 µg/ml) as indicated by the manufacture.

2.1.2 HL-1 cell culture

HL-1 cells, a murine cell line with an atrial-like phenotype was cultured in Claycomb medium (SAFC Bioscience, USA) supplemented with fetal bovine serum (FBS) (10%), L-glutamine (2 mmol/L), and norepinephrine (0.1 mmol/L) as described below.

Pre-coating culture flasks with gelatin/fibronectin

A vented T25 flask was typically coated with a gelatin/fibronectin solution (0.02 % gelatin/0.1 % fibronectin) before plating and culture of *HL-1* cells. For coating, 2.5 ml of the solution was added to the flask and incubated for 2-3 hr at 37°C prior to the addition of the HL-cells. The solution was then aspirated and the flask was washed once with 5 ml of phosphate buffered saline (PBS) prior to the addition of the culture medium and cells. To prepare a 0.02 % gelatin solution, 80 mg of gelatin from bovine skin (Sigma-Aldrich; G9391) was added to 400 ml of cell culture grade water and autoclaved for 30 min. After cooling to room temperature, 2 ml of a sterile 1 mg/ml fibronectin solution (Sigma-Aldrich; F-1141) was added and mixed. Aliquots were frozen and stored until used for coating of the flask.

Cell maintenance and passaging

Cultured HL-cells were maintained with 6.0 ml/flask of complete Claycomb medium changed daily with an every other day subculture cycle. Confluent flasks were then passed into subcultures. This was carried out by carefully rinsing the T25 flask containing a confluent layer of *HL-1* cells, with 3 ml PBS warmed to 37°C. After gently rinsing the cells, PBS was removed by aspiration. To gently dissociate the confluent cell layer, 1 ml of 0.05 % trypsin/EDTA was added to the T25 flask and incubated for 1 min at 37°C. The trypsin/EDTA after 1 min was aspirated and again 2 ml of trypsin/EDTA was added and the cells were incubated for an additional 2 min. Following this step 1.5 ml of soybean trypsin inhibitor was directly added onto the cells so as to inactivate the trypsin enzyme activity. The flask was next tapped forcefully to dislodge the cells. The contents of the flask was pipetted and transferred to a 15 ml centrifuge tube. A pellet of *HL-1* cells was obtained by centrifuging the contents in the tube at 500 rpm for 5 min. A pre-coated T25 flask was then prepared as described above for cell plating. Excess fibronectin/gelatin solution was aspirated and 6 ml of supplemented Claycomb medium was added to each flask. After centrifugation of the cells, the supernatant was aspirated and the pellet was gently re-suspended in 6 ml of supplemented Claycomb media. The pellet was gently broken down by pipetting the entire contents of the tube up and down a couple of times. Once the cells were mixed in the medium, 3 ml was transferred to each T25 flask. The flasks are then placed in an incubator at 37°C for culturing. To maintain the cell culture, 6 ml of supplemented Claycomb medium was routinely replaced with fresh medium daily in the flasks.

2.2 Multi-electrode arrays

2.2.1 Theory

Multi-electrode arrays (MEAs) are devices that consist of an array of microelectrodes arranged in fixed geometrical configurations and used for simultaneous, multisite extracellular

electrophysiological recordings from excitable cells such as neurons and cardiomyocytes. Excitable cells cultured on the MEAs make point contact with the planar electrodes and their spontaneous or stimulated depolarization is recorded as an extracellular field potential by the electrodes of the MEA in real-time. It has been previously demonstrated that the rise time and duration of the generated intracellular cardiac action potential is linearly correlated with the rise time and duration of the extracellular field potentials detected using MEAs [68]. The electrical coupling between the cell and the electrode enables this detection of field potential. Figure 3 depicts the cell-electrode coupling.

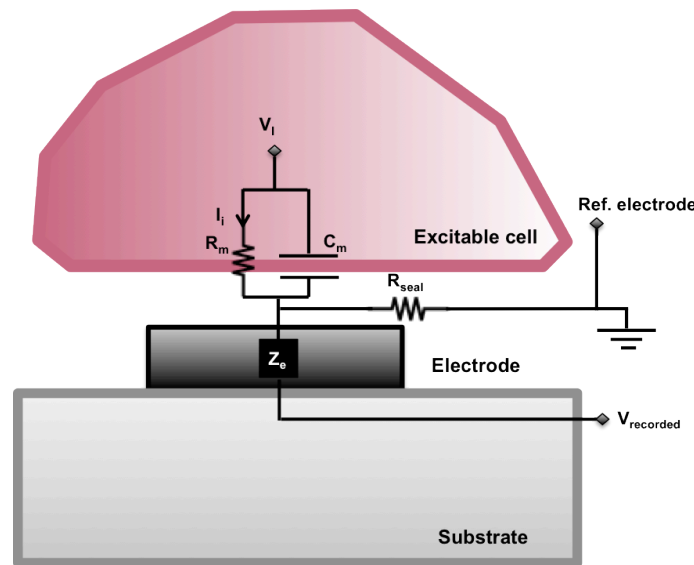


Figure 3: A pictorial representation of the electrical coupling between a cell and a planar electrode. V_i is the intracellular potential, R_m and C_m is the resistance and capacitance of the cell membrane respectively, I_i is the ionic current across the cell membrane, R_{seal} is the sealing

resistance between the electrode and the cell, Z_e is the impedance of the electrode and V_{recorded} is the output field potential recorded against the reference electrode by the signal detection system (Adapted with permission from [69]).

In excitable cells, the movement of ions across the membrane generates a change in membrane voltage accompanied by changes in both intracellular (V_i) and extracellular potential. The change in membrane voltage modifies the electric field between the electrode and the electrolyte interface thereby producing a voltage change at the electrodes. This voltage change is recorded as extracellular field potential (V_{recorded}). The seal resistance (R_{seal}) determines the amount of leakage current produced at the interface between the electrode and the cell and is inversely proportional to the electrode area, i.e. the smaller the electrode, the greater is the seal resistance and lower is the leakage current. The field potential thus recorded is then used for computing electrophysiological parameters such as conduction velocity and beating frequency (described in Fig. 4).

2.2.2 Multi-electrode array recordings

To monitor excitation spread in spontaneously active *HL-1* monolayers the cells (0.3×10^6 cell/ml) were plated on multi-electrode arrays (MEAs; Multi Channel Systems, Reutlingen, Germany) for field potential recordings [38, 68, 70, 71]. For co-culture assays, 0.2×10^6 MSCs were added to the *HL-1* monolayers and electrophysiological changes were determined in 30 min intervals. MEAs consisted of 60 electrodes arranged in 8x8 matrix each with a diameter of $\varnothing = 30 \mu\text{m}$ and an inter-electrode distance of $200 \mu\text{m}$. They were coated with 0.1 % fibronectin (1 mg/ml, Sigma Aldrich) for 4 h prior to plating. Experiments were conducted at 37°C and data acquisition and analysis was performed using Cardio 2D and Cardio 2D+ software (Multi Channel Systems, Reutlingen, Germany), respectively. The Cardio 2D software was used to

record and run experiments. The Cardio 2D+ analyzer was used for analyzing and reviewing the recorded experiments. The raw data were recorded in 16-bit resolution at a sampling rate of 10 kHz. Figure 5 shows a screenshot of the field potentials recorded simultaneously in all 60 electrodes in the MEA using Cardio 2D software. Negative voltage deflections seen in each field potential recording represent the action potentials generated by the cardiomyocytes.

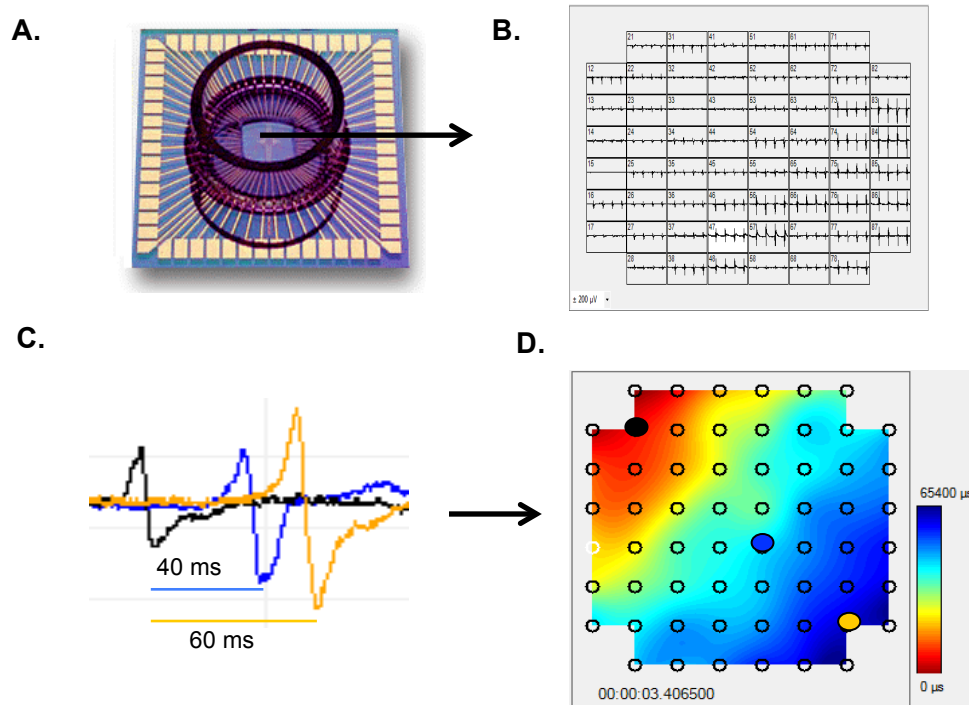


Figure 4: Field potential recordings using multi-electrode arrays. Field potentials are recorded simultaneously from all 60 electrodes in the MEA (A) using Cardio 2D software (B). Field potentials appear with a delay on the different electrodes reflecting the propagation of APs through the cardiomyocytes monolayer (C). This delay can be presented as a contour plot

where the color-coded excitation wave front indicates the time delay across the electrodes (D). The conduction velocity (θ) is calculated in the direction perpendicular to the excitation wave-front.

The two parameters analyzed in this study were the conduction velocity (θ) and the spontaneous beating frequency. Both were obtained from the software using the recorded data. Conduction velocity is computed in the direction perpendicular to the wave front propagation by dividing the distance between any two electrodes by the time delay existent between the field potentials recorded from these electrodes. This information is recorded by the Cardio 2D software in real time and later used to calculate the θ .

We report θ as percent change, which was calculated using the following formula:

$$\% \text{ Change in } \theta = \frac{(\theta_{xh} - \theta_{0h}) \text{ cm/s}}{\theta_{0h} \text{ cm/s}} \quad (1.1)$$

where θ_{xh} is the velocity at 1.0 – 4.0 h and θ_{0h} is the velocity at 0h in (1.1)

2.2.3 Electrophysiological recordings evaluating conditioned media/tyrode

Evaluation of ConM was done by replacing half the culture medium with ConM (400 μ L) in the MEA having a total volume of 800 μ L. Electrophysiological recordings were made in 60 min intervals for an experimental window of 5 h. Dr. Christopher Gans carried out the experiments evaluating ConM. For experiments evaluating ConT, the culture medium on each MEA (800 μ L) was replaced by Ctrl tyrode solution in order to establish baseline activity. After 30 min cells were transferred either to Ctrl or ConT for the duration of the experiment (4 h) and

recordings were made in 30 min intervals. A total of two recordings in 2 min intervals were made for each time point.

2.3 Conditioned medium/Tyrode preparation

For Conditioned tyrode (ConT) production, only MSCs at passage 8 or 9 were utilized and were plated at a density of 300,000 cells per 100 mm tissue culture plate and maintained until they were approximately 80 % confluent. The plated MSCs were then carefully washed twice with 5 ml of tyrode solution (in mmol/L: NaCl 130, KCl 5.4, CaCl₂ 1, MgCl₂ 1.5, NaHCO₃ 10, Glucose 10, Hepes 25, L-glutamine 4, non-essential amino acids 0.1; pH 7.4) (28) warmed to 37°C followed by the addition of a final 10 ml of tyrode and returned to the incubator (37°C, 5% CO₂) for an overnight incubation (15 h). The following morning the tyrode was recovered from each plate with pipetting and transferred to a sterile 50 ml conical centrifuge tube for low-speed centrifugation. The ConT was then centrifuged at approximately 2,000-x g for 15 min to remove large cellular debris and the supernatant was carefully recovered. Finally, aliquots of ConT were made in 10 ml centrifuge tubes and frozen by placing them directly into -80°C storage. Human MSCs were obtained from Dr. D.J. Prockop's laboratory (Texas A&M, Institute for Regenerative Medicine) and cultured as previously described [72]. Human ConT (ConT_h) was prepared in the same manner as ConT obtained from mouse MSCs.

To obtain the conditioned medium (ConM), the MesenCult® medium was aspirated from confluent 100 mm plates of MSCs and replaced with Claycomb base medium (Sigma-Aldrich; St. Louis, MO) supplemented with 2 mmol/L L-glutamine and penicillin/ streptomycin (50 U/ml/ 50 µg/ml) for an overnight incubation. Dr. Dan J Bare routinely carried out the ConT production and Dr. Christopher Gans prepared the ConM used for this study.

2.4 Co-culture and dye diffusion assay

To determine the time course of intercellular coupling between *HL-1* cells and MSCs, MSCs were loaded with calcein acetoxymethyl ester (Calcein AM, 2.5 $\mu\text{mol/L}$, 60 min at 37°C; Invitrogen) and Vybrant-DiD (2.5 $\mu\text{mol/L}$, 30 min at 37°C; Invitrogen) in serum free Dulbecco's modified eagle medium (DMEM) and 200 $\mu\text{mol/L}$ probenecid (Sigma) [73]. Dye loaded MSCs (0.3×10^6) were transferred to *HL-1* monolayers grown on glass-bottom tissue culture dishes. Dye diffusion between MSCs and *HL-1* cells was monitored by confocal microscopy and analyzed using ImageJ [National Institutes of Health, Bethesda, MD] [38]. Data were analyzed as the percentage of MSCs coupled to *HL-1* cells per optical field. Dr. Christopher Gans carried out this experiment for the study.

2.5 Quantitative reverse transcriptase polymerase chain reaction

Total RNA was isolated from MSCs or *HL-1* cells using the RNeasy Mini Kit (Qiagen, USA) according to the manufacturer's protocol. Total RNA was treated with DNAase I (Fermentas Life Sciences, USA) to remove residual genomic DNA. Treated total RNA was then used as template for complementary DNA (cDNA) synthesis using the RevertAid First Strand cDNA Synthesis Kit (Fermentas Life Sciences, USA). The cDNA synthesis reaction was performed using random hexamer primers supplied by the manufacturer. cDNA was used as template in quantitative PCR reactions with gene-specific primers and SYBR Advantage qPCR premix (Clontech, USA). The primer 18S was used for normalization (5'AATTGACGGAAGGGCACCAC3'; 5'GTGCAGCCCCGGACAT CTTAAG3'). A primer set spanning the intron of connexin 46 (Cx46) (5'GGTGGTGGTGGTGGTAAAAG3'; 5'CTACTGGGGAGAGCAGGACA3') served as a negative control for genomic DNA contamination. Expression of target genes was normalized to expression of 18S using QGene software (21). Cx43 (5'TCCAAGGAGTTCCACCACTT3';

5'GGACCTTGTCC AGCAGCTT3') and Cx45 (5'TGGGTAACAGGAGTTCTGGTG3'; 5'CAAATGTCTG AATGGTTGTGG3') primer sets were verified to amplify cDNA synthesized from known positive tissues (data not shown). This work was carried out by Dr. Christopher Gans.

2.6 Pharmacological treatment of *HL-1* cells

LiCl (5 mmol/L; Sigma-Aldrich), an inhibitor of GSK-3 β [74] was added to both Ctrl and ConT treated *HL-1* monolayers. To achieve a 5 mmol/L concentration of LiCl in the MEA, 4 μ L of 1M LiCl was added to each MEA having a final volume of 800 μ L. Recordings were made in 30 min intervals after the addition of LiCl to the MEAs.

Cardamonin (10 μ mol/L; EMD-Millipore), an inhibitor of β -catenine [75] was added to both Ctrl and ConT treated groups. A final concentration of 10 μ mol/L of cardamonin was achieved in each MEA by adding 3.3 μ L of the 15 mmol/L stock solution to a final volume of 800 μ L. Recordings were made in 30 min intervals after the addition of cardamonin to the MEAs. Treatment of Ctrl and ConT-treated *HL-1* monolayers with vascular endothelial growth factor receptor-2 (VEGF R2/Flk-1) antibody was carried out by adding 5 μ L of the VEGF R2 antibody stock solution to each MEA to achieve a final concentration of 1 μ g/ml [64]. Electrophysiological recordings were made in 30 min intervals as previously described.

Suppression of Wnt production and release by MSCs was carried out using a small molecular inhibitor of the canonical Wnt pathway known as IWP-2 [76]. MSCs were treated with 5 μ mol/L of IWP-2 for 24 h for this purpose before the tyrode was added for conditioning in their presence (ConT_{IWP-2}). The final concentration of IWP-2 in ConT_{IWP-2} was 0.5 μ mol/L. This ConT_{IWP-2} was then used to treat the *HL-1* monolayers plated on MEAs for duration of 4 h. PD98059 (25 μ mol/L Cell Signaling Technology), an inhibitor of ERK1/2 [77] was used to treat

the Ctrl and ConT treated HL-1 monolayers. A 20 mmol/L stock of PD98059 was pre-mixed with both the Ctrl and ConT solutions in a ratio of 1:800 μ L and then added to each MEA to equal a final concentration of 25 μ mol/L. Electrophysiological recordings were made in 30 min intervals as previously described.

Wnt3a, an activator of the canonical Wnt-signaling pathway was obtained from Wnt3a overexpressing L-cells [78] in the form of Wnt3a conditioned media from Dr. Merrill's laboratory. This Wnt3a conditioned media was used to treat the spontaneously active *HL-1* monolayers. Wnt3a conditioned media was added along with the Claycomb media on the MEAs in the ratio of 1:1. Electrophysiological recordings were made in 30 min intervals after the addition of the Wnt3a.

2.7 SDS-PAGE and western blotting

100% confluent HL-1 cells plated on 35-mm tissue culture dishes were recovered following experimental treatment (0.5 or 4 h) with the addition of hot 1-X Laemmli sample buffer lacking β -mercaptoethanol (β -ME) and bromophenol blue dye. The samples were then heated to 95°C for 5 min and stored at -20°C until further processing. Sample protein determinations were made with a BCA protein assay kit (Pierce) followed by the addition of β -ME and dye to the final concentrations appropriate for the 1-X sample buffer and heated as before. The HL-1 cell lysates were separated for protein analysis using either pre-cast 10 % or 4-20 % Novex tris-glycine gels (Invitrogen) following standard electrophoresis protocols for SDS-PAGE and western blotting. Typically, 35 μ g of protein was loaded per sample however, for the detection of phospho-LRP6 120 μ g of total protein was required. Primary antibodies used for western blotting were anti- phospho-Akt-Ser473 (#4058), phospho-ERK1/2 (#4370), phospho-LRP6-Ser1490 (#2568), GAPDH (#5174) from Cell Signaling Technology, anti-connexin 43 (71-0700; Invitrogen) and anti- β -catenin (C7207; Sigma-Aldrich). Species-specific horseradish peroxidase-

conjugated secondary antibodies were used and visualization was accomplished using Western Lighting Plus-chemiluminescence reagents (PerkinElmer) and Kodak BioMax film. Dr. Dan J Bare did all western blotting.

2.8 Statistical Analysis

Experimental values were compared to controls using the unpaired two-tailed Student's t test. Non-linear regression was performed using GraphPad Prism software. Data are presented as mean \pm SEM. Absolute and percent change values for θ and beating frequency are presented in the text. Differences were considered significant at $P < 0.05$.

3. RESULTS

3.1 Mesenchymal stem cells modulate the spontaneous activity of *HL-1* cells

It has been demonstrated that non-excitabile cells such as fibroblasts change the spontaneous activity of cardiomyocyte monolayers [38, 79]. To determine the influence of MSCs on the electrophysiological properties of multicellular cardiomyocyte preparations monolayers of *HL-1* cells were established on MEAs. After 1 day in culture *HL-1* monolayers exhibited a typical spontaneous beating frequency of 2.26 ± 0.18 Hz ($n = 10$) and a conduction velocity (θ) of 1.5 ± 0.15 cm/s ($n = 4$). At this time 0.2×10^6 MSCs dissociated in MSC medium were added to the MEA. In Ctrl MEAs the beating frequency of the *HL-1* monolayers exhibited a slight increase over time in culture ($t_{5h} = 2.92 \pm 0.34$ Hz; $n = 4$) while cultures supplemented with MSCs exhibited a decrease in beating frequency, starting 2 h after co-culture (Fig. 5A). After 5h the frequency decreased to t_{5h} : 1.98 ± 0.26 Hz ($n = 7$) or 0.82 ± 0.09 when normalized to the frequency at t_0 and was significantly reduced compared to time matched homo-cellular *HL-1* monolayers (t_{5h} : 1.22 ± 0.06 , $n = 4$; $p < 0.01$). The MSC-mediated suppression of the spontaneous activity was also reflected in the increased likelihood of cessation of beating in the cultures (not shown). In *HL-1* MEAs at t_{5h} cessation of spontaneous activity was observed in only 14.8 % of the cultures. Some *HL-1*/MSC-MEAs however stopped beating already after t_{3h} of co-culture, with 71.3 % of the cultures quiescent at t_{5h} .

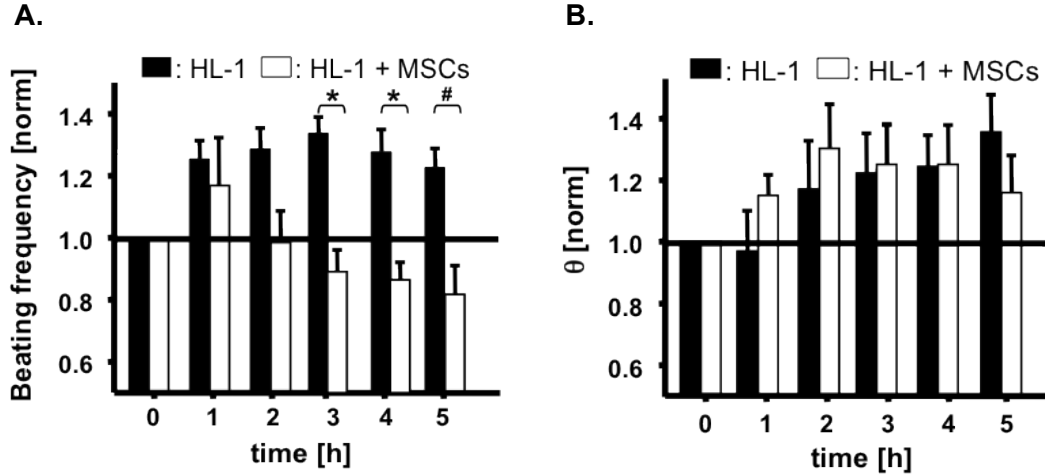


Figure 5: MSCs modify the electrophysiological properties of cardiomyocytes: Addition of MSCs to a monolayer of spontaneously beating *HL-1* cells attenuates the beating frequency over time (A) while no change in θ was determined (B) (*, # $p < 0.05$ compared to *HL-1*) [80].

3.2 *HL-1* cells and mesenchymal stem cells establish intercellular coupling via gap junctions

Others and we have previously demonstrated that non-excitabile cells like fibroblasts can change cardiomyocyte excitability by establishing hetero-cellular coupling through gap junction channels [38, 79]. To determine if and in which time frame the spontaneous beating rate of *HL-1* cells is altered by hetero-cellular coupling with MSCs, we plated calcein AM loaded MSCs onto a monolayer of *HL-1* cells. Hetero-cellular coupling was identified when calcein fluorescence was detected in *HL-1* cells and a dye loaded MSC was identified on top of the monolayer (Fig. 6A). Intercellular dye diffusion was detected as early as 20 min after co-culture was established and the number of coupled cells increased over the initial 4 h (Fig. 6B: t_{4h} : 46.23 ± 2.99 %; $n = 13$ cultures with a total of 570 cells analyzed) while only a gradual increase in the number of coupled cells was determined after that (t_{24h} : 60.07 ± 4.8 %; $n = 13$). Dye diffusion

between MSCs and *HL-1* cells was significantly attenuated when the co-culture was established in the presence of the gap junction inhibitor carbenoxolone (100 μm ; $t_{4\text{h}}$: 1.75 ± 1 %; $n = 3$). The results support the hypothesis that the hetero-cellular coupling established between MSCs and *HL-1* cells changes the spontaneous beating rate of the *HL-1* monolayer thereby demonstrating that it is attributed primarily to hetero-cellular coupling.

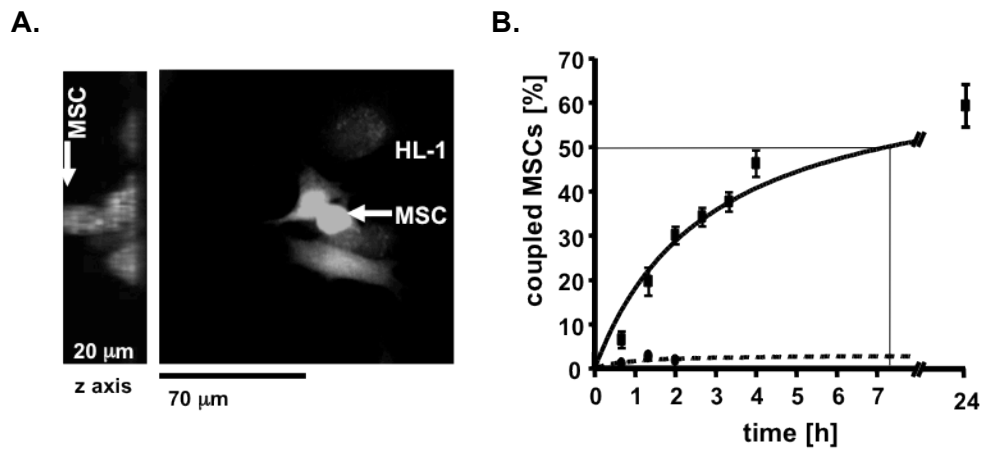


Figure 6: MSCs establish inter-cellular coupling with cardiomyocytes: 3D-reconstruction of z-stack images (A, left) obtained by confocal imaging shows calcein/AM loaded MSCs on top of an *HL-1* monolayer (A, right). Dye transfer through gap junction channels was determined between the two cell types. Hetero-cellular coupling between MSCs and *HL-1* cells occurs rapidly over the first hours of co-culture (B; solid line) and is suppressed by carbenoxolone (B; dotted line) [80].

Homo- and hetero-cellular *HL-1* monolayers exhibited a gradual increase in θ over time (t_{5h} : *HL-1*: 1.9 ± 0.1 cm/s, $n = 4$; *HL-1/MSC*: 1.6 ± 0.16 cm/s, $n = 6$) representing a 1.35 and 1.16 fold increase, respectively over a 5 h period ($p < 0.3$). No significant difference of θ was determined between homo- and hetero-cellular cultures at any time of the experiment (Fig. 5B). This result was in contrast to our previous experiments using hetero-cellular cultures of *HL-1* cells and fibroblasts where intercellular coupling induced a decrease in θ [38].

To test the hypothesis that paracrine factors secreted by MSCs compensate for the coupling induced decrease in θ we treated *HL-1* monolayers with either MSC culture media (ConM: Fig. 7A), or tyrode that was conditioned by mouse or human MSCs [61] (Fig. 7B). Neither ConM (ConM: t_{0h} : 2.41 ± 0.11 Hz; t_{4h} : 2.46 ± 0.07 Hz; $n = 17$), mouse ConT (ConT: t_{0h} : 3.34 ± 0.37 Hz; t_{4h} : 3.93 ± 0.27 Hz; $n = 13$) or human ConT (ConT_h: t_{0h} : 2.776 ± 0.293 Hz; t_{4h} : 2.844 ± 0.523 Hz; $n = 5$) induced a change in the spontaneous beating of the *HL-1* monolayers in comparison to Ctrl cultures (Ctrl: t_{0h} : 4.13 ± 0.19 Hz; t_{4h} : 4.17 ± 0.16 Hz; $n = 27$). However, in contrast to *HL-1/MSC* co-cultures, treatment of *HL-1* monolayers with ConM (ConM: t_{0h} : 1.2 cm/s ± 0.05 ; t_{4h} : 1.9 ± 0.1 cm/s; $n = 17$; $p < 0.05$), ConT (ConT: t_{0h} : 1.84 ± 0.57 cm/s; t_{4h} : 2.93 ± 0.74 cm/s; $n = 13$; $p < 0.05$) or ConT_h (ConT_h: t_{0h} : 1.08 ± 0.07 cm/s; t_{4h} : 1.57 ± 0.18 cm/s; $n = 5$; $p < 0.05$) significantly increased θ over time (Fig. 7A,B). No significant change was determined in *HL-1* monolayers that were treated with media or tyrode alone (*HL-1* + tyrode: t_{0h} : 1.49 ± 0.33 cm/s; t_{4h} : 1.72 ± 0.49 cm/s; $n = 26$). The results support the hypothesis that paracrine factors secreted by MSCs modulate cardiac conduction velocity.

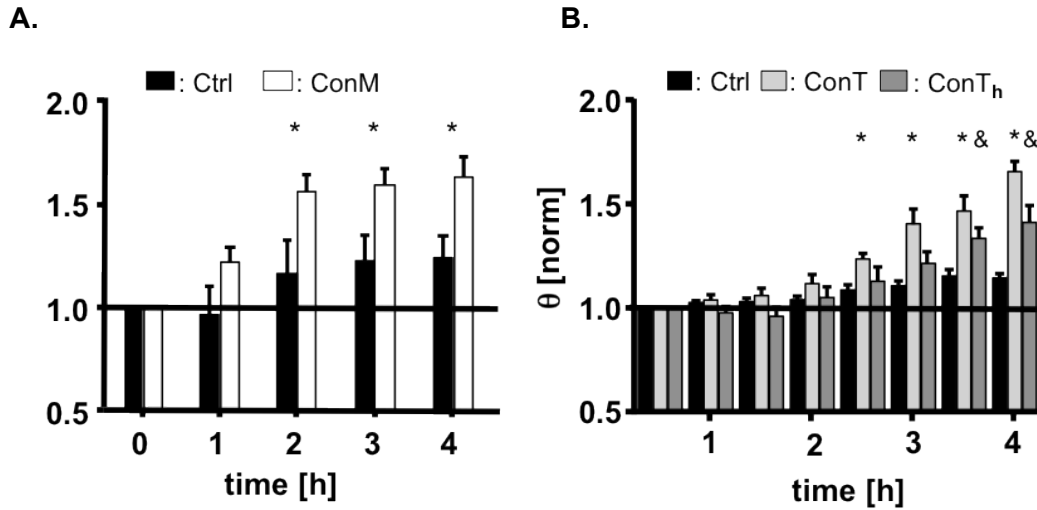


Figure 7: Paracrine factors secreted by MSCs increase the conduction velocity of *HL-1* monolayers. Conditioned culture medium from MSCs (ConM, A) as well as tyrode conditioned in the presence of mouse MSCs (ConT, B) and human MSCs (ConTh, B) increased θ in *HL-1* monolayers in a time-dependent manner (*, &: $p < 0.05$ compared to Ctrl) [80].

An increase in θ of cardiomyocyte monolayers can be induced by enhanced depolarizing currents that drive the upstroke of the action potential (AP) or a decrease in the intercellular resistance due to an increased number of gap junction channels. To determine the contribution of the voltage dependent sodium current (I_{Na}) to changes in θ we increased the extracellular potassium $[K]_o$ from 4.8 mmol/L to 8.5 mmol/L [71] in cultures that were treated with ConM for 4 h. In Ctrl and ConM treated *HL-1* monolayers (not shown) the increase in $[K]_o$ resulted in a decrease of the beating frequency compared to t_0 (Ctrl: t_{4h} : 24.2 ± 6.3 %, $n = 4$; ConM: t_{4h} : 20.3 ± 6.5 %, $n = 5$). While θ was decreased for Ctrl preparations over time, it remained significantly increased in ConM treated *HL-1* monolayers (Ctrl_K: 0.8 ± 0.07 cm/s, $n = 4$; ConM_K: 1.4 ± 0.1

cm/s, $n = 5$; $p < 0.01$). In addition, no changes in protein level of Nav1.5 were determined after 4h treatment with either ConM (Fig. 8C) or ConT (Fig. 8D). The result supports the hypothesis that paracrine signaling from MSCs increases θ by a mechanism independent of I_{Na} .

To determine if MSC secreted factors enhance the intercellular coupling, we determined the expression of cardiac connexin isoforms in control and ConM treated *HL-1* monolayers by qRT-PCR. In accordance with their atrial phenotype, mRNA for Cx40, Cx43 and Cx45 was confirmed in HL-1 cells [71]. Cx43 was expressed at the highest abundance (8-fold higher levels than Cx45). After 4 h treatment of *HL-1* cells with ConM, Cx43 mRNA levels were significantly increased in comparison to Ctrl treated cells (Cx43: 1.829 ± 0.243 ; $n = 3$; $p < 0.05$). The effect was specific to Cx43 and no change in Cx45 mRNA was determined (Cx45: 1.322 ± 0.115 , $n = 3$; Fig. 8A). The increase in Cx43 mRNA was also reflected in the protein level. Immunoblotting of whole cell lysates revealed an increase in Cx43 protein after 4h treatment of *HL-1* cells with either ConM (Fig. 8C) or ConT (Fig. 8D). Densitometric analysis of the western blots (Fig. 8B) showed a small but significant increase in the ratio of phosphorylated vs. non-phosphorylated Cx43, over the 4h time period. Induction of Cx43 expression has been described downstream of the glycogen synthase kinase-3 (GSK-3)/ β -catenin signaling cascade [65].

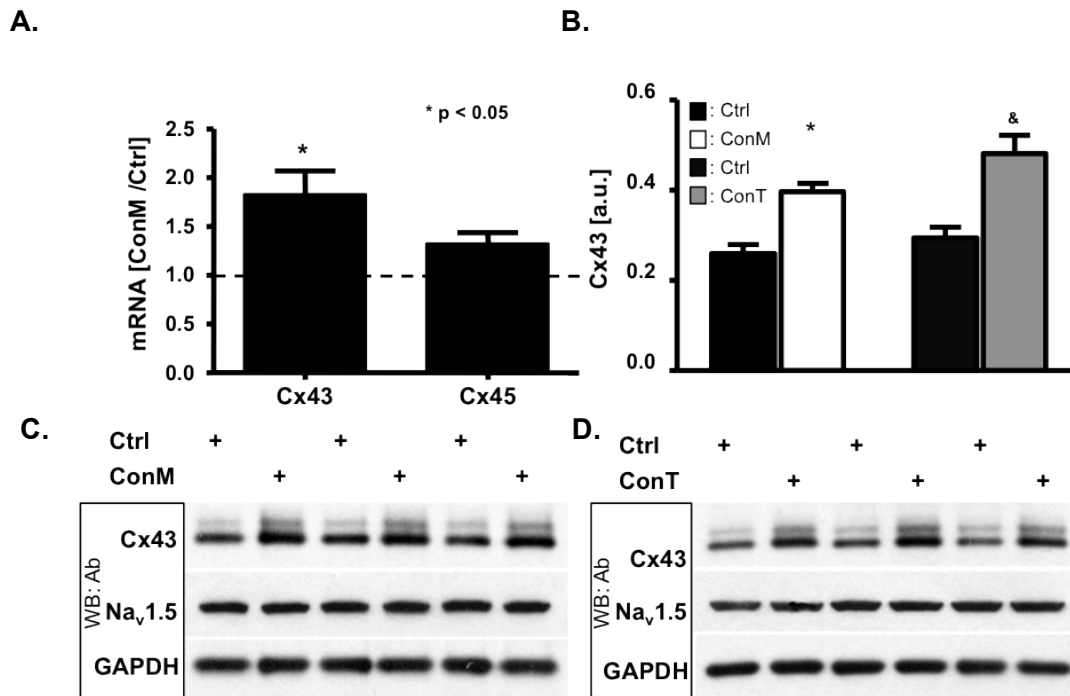


Figure 8: MSC-conditioned medium increases Cx43 expression in cardiomyocytes. mRNA content of Cx43 and Cx45 determined by quantitative RT-PCR in HL-1 cells after 4 h of treatment with ConM showed a significant increase in Cx43 but not Cx45 (A). Densitometric quantitation of Cx43 blots (B) shown in (C, D), revealed a significant increase in the ratio of phosphorylated vs. non-phosphorylated Cx43 in both ConM and ConT-treated groups (*, &: $p < 0.05$ compared to respective Ctrl). Western blotting results of ConM (C) and ConT (D) treated HL-1 cells probed for Cx43 and Na_v1.5 protein levels. GAPDH is shown as a loading control (n = 3 for each group) [80].

To evaluate if β -catenin signaling is required for the increase in θ we supplemented ConT with cardamonin (10 μ mol/L). Cardamonin that was previously described to stabilize β -catenin in its degradation complex [81] significantly attenuated the ConT-induced increase in Cx43 protein expression and θ (ConT+carda: t_{4h} : 1.52 ± 0.20 cm/s, $n=7$; ConT: t_{4h} : 2.52 ± 0.20 cm/s, $n=8$; $p < 0.05$) (Fig. 9 A, B). In Ctrl cultures supplemented with cardamonin also a slight reduction in Cx43 protein levels was determined however, without a significant change in θ . The results support the hypothesis that ConT regulates Cx43 and concomitant changes in θ through stimulation of β -catenin signaling.

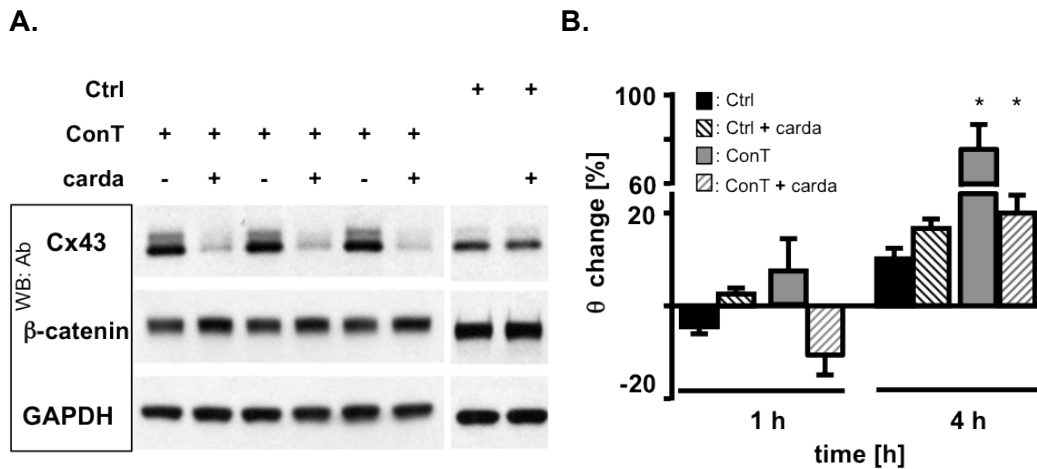


Figure 9: β -Catenin inhibition prevents the ConT-mediated increase in Cx43 protein levels: Western blotting analysis of Cx43 protein levels (A) after 4 h of ConT or Ctrl treatment in the presence or absence of cardamonin ($n = 3$ for each). Cardamonin prevented the ConT-mediated increase of θ in *HL-1* monolayers (B)(*: $p < 0.05$ compared to Ctrl) [80].

3.3 ConT-mediated upregulation of connexin 43 depends on β -catenin and glycogen synthase kinase 3- β

β -catenin is a downstream target of GSK3- β , a serine/threonine kinase that phosphorylates and stabilizes β -catenin in its degradation complex [82]. Phosphorylation and consequently the inactivation of GSK3- β is regulated by different signal-transduction pathways, including a PI3K/Akt and a Wnt-dependent signaling cascade [83]. To determine if inhibition of GSK3- β can mimic the ConT mediated effect we supplemented Ctrl solution and ConT with lithium (LiCl, 5 mmol/L) an inhibitor of GSK3- β . Addition of LiCl to Ctrl solution induced a time-dependent increase in θ (Fig. 10B: Ctrl_{Li}: t_{4h} : 2.67 ± 0.07 cm/s; , $n = 7$; $p < 0.05$) and increased Cx43 protein levels (Fig. 10A); the addition of LiCl to ConT on the other hand did not have an additive effect (ConT_{Li}: t_{4h} : 2.90 ± 0.13 cm/s; $n = 10$; ConT: t_{4h} : 2.93 ± 0.20 cm/s; $n = 13$), indicating that ConT and LiCl converge on the same downstream signaling mechanism.

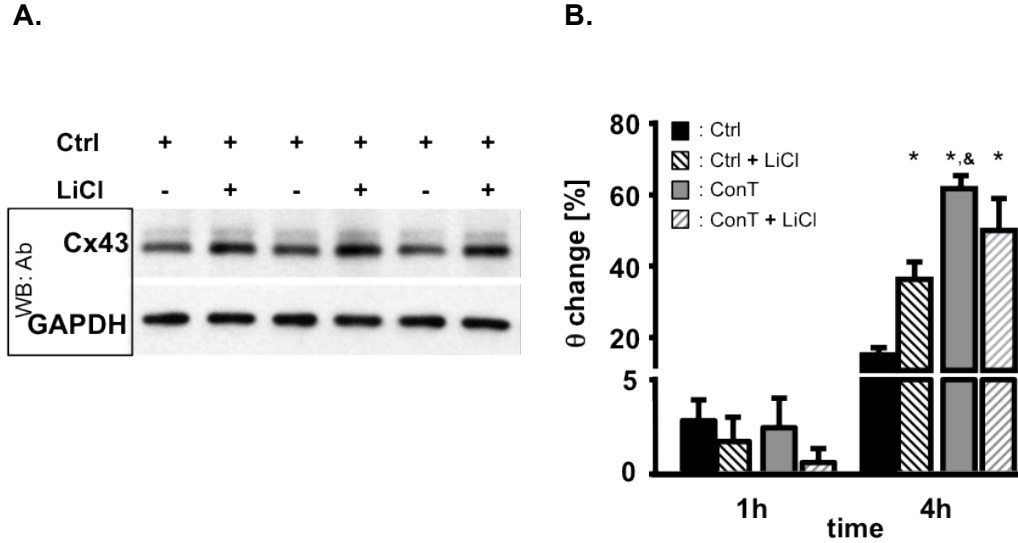


Figure 10: Lithium inhibition of GSK-3 β mimicks the effect of ConT on θ and Cx43 protein expression. Supplementation of Ctrl tyrode with LiCl (4 h) led to an increase in Cx43 protein levels in *HL-1* monolayers (A). A concomitant increase in θ (B) was seen in spontaneously beating *HL-1* cells. The LiCl induced increase in θ was not additive to the effect of ConT (*: $p < 0.05$ compared to Ctrl; &: compared to Ctrl + Li) [80].

We have previously demonstrated that ConT induces GSK3- β phosphorylation through the PI3K/Akt pathway in isolated mouse ventricular myocytes [61]. Since PI3K/Akt is a downstream target of VEGF signaling we determined its role in the regulation of Cx43 expression. However, supplementation of ConT with the PI3K inhibitor Wortmannin (WM: 50-100 nmol/L, Fig.11A), or supplementation of ConT with a VEGF R2/Flk-1 antibody (1 μ g/ml)[64] (ConT+anti-VEGFR: t_{4h} : 2.33 ± 0.13 cm/s; $n=4$; ConT: t_{4h} : 2.93 ± 0.20 cm/s; $n=13$) (Fig. 11C) did not prevent the ConT induced upregulation of Cx43 or an increase of θ in *HL-1* cells, respectively.

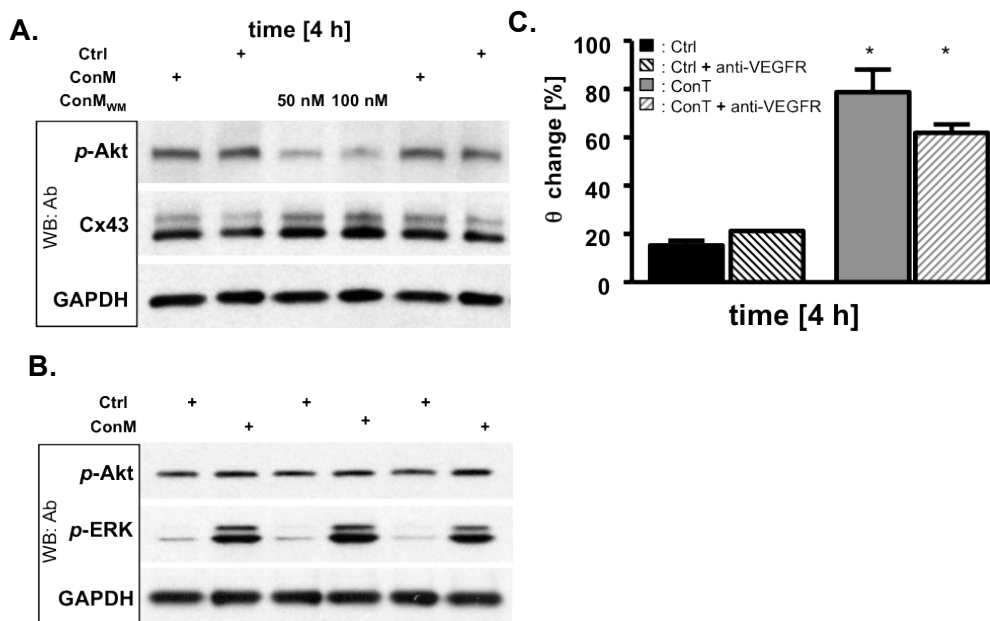


Figure 11: A ConM-mediated increase in θ does not depends on PI3K/Akt signaling. Western blotting analysis of ConM-mediated (4 h) changes in *p*-Akt and Cx43 in the presence and absence of Wortmannin (WM: 50 and 100 nM)) (A). ConM (4 h) also increased *p*-ERK 1/2 while changes in *p*-Akt were close to baseline (B). GAPDH is shown as a loading control for both experiments. The change of θ in Ctrl and ConT treated *HL-1* cells with and without the addition of an anti-VEGF receptor (anti-VEGFR) antibody (*: $p < 0.05$ compared to Ctrl) (C) [80].

GSK3- β phosphorylation is also a downstream target of the canonical Wnt pathway after stimulation of the frizzled receptor. To identify if ConT activates Wnt receptor signaling we determined the phosphorylation levels of low-density lipoprotein receptor-related protein 6 (LRP6). LRP6 is part of the Wnt receptor and becomes phosphorylated upon Wnt stimulation

[84]. In ConT-treated *HL-1* cells (30 min) the LRP6 phosphorylation level was increased (Fig. 12A). To suppress the release of Wnt, MSCs were treated with the small molecule inhibitor of the Wnt pathway IWP-2 (5 $\mu\text{mol/L}$, 24 h) before tyrode was conditioned in their presence (ConT_{IWP-2}). The final concentration of IWP-2 in ConT_{IWP-2} was 0.5 $\mu\text{mol/L}$. When *HL-1* cells were treated with ConT_{IWP-2}, LRP6 phosphorylation was significantly reduced compared to ConT treated cells (Fig. 12A, B). After 4h of incubation, Cx43 expression was not significantly different from ConT treated *HL-1* cells (Fig. 12C) however the ConT induced increase in θ was attenuated (ConT_{IWP-2}: t_{4h} : 1.80 ± 0.05 cm/s, $n=7$; ConT: t_{4h} : 2.73 ± 0.19 cm/s, $n = 16$; $p < 0.05$) (Fig. 12D) [80].

It was previously demonstrated by mass spectroscopy studies and RNA expression profiling that Wnt3a is expressed in MSCs [85]. To determine if Wnt3a can mimic the same effect, media from Wnt3a over-expressing L-cells [78] was added to *HL-1* monolayers (Fig. 13A, Ctrl + Wnt3a). Also in this case an increase in θ compared to non-treated Ctrl cultures was determined (Ctrl + Wnt3a: t_{4h} : 1.88 ± 0.18 cm/s, $n=6$; Ctrl: t_{4h} : 1.85 ± 0.11 cm/s, $n = 4$; $p < 0.05$) (Fig. 14A). These results support the hypothesis that MSC ConT-induced changes are in part through activation of the canonical Wnt pathway. However, with significant LRP6 phosphorylation remaining in ConT_{IWP-2} another mechanism of LRP activation remained likely. Particularly since the IWP-2 concentration used was previously shown to predominately block Wnt secretion [86]. Recent evidence indicates the MAP kinases ERK1/2 in an alternative pathway of LRP6 phosphorylation [87]. We evaluated ERK1/2 activity in *HL-1* lysates and found that both ConM and ConT significantly increased ERK1/2 phosphorylation at 30 min and 4.0 h of incubation (Fig. 11B, 12A,B). Supplementation of ConT with the ERK1/2 inhibitor PD98059 (25 μ mol/L) [88] significantly attenuated the ConT-mediated increase in θ (ConT + PD98059: t_{4h} : 2.04 ± 0.11 cm/s, $n = 4$; $p < 0.05$) (Fig. 14B) no change was determined in Ctrl cultures with PD98059 (Ctrl + PD98059: t_{4h} : 1.41 ± 0.03 cm/s; $n = 3$). These results strongly suggest that *p*-ERK 1/2 can contribute to GSK3/ β -catenin mediated Cx43 upregulation.

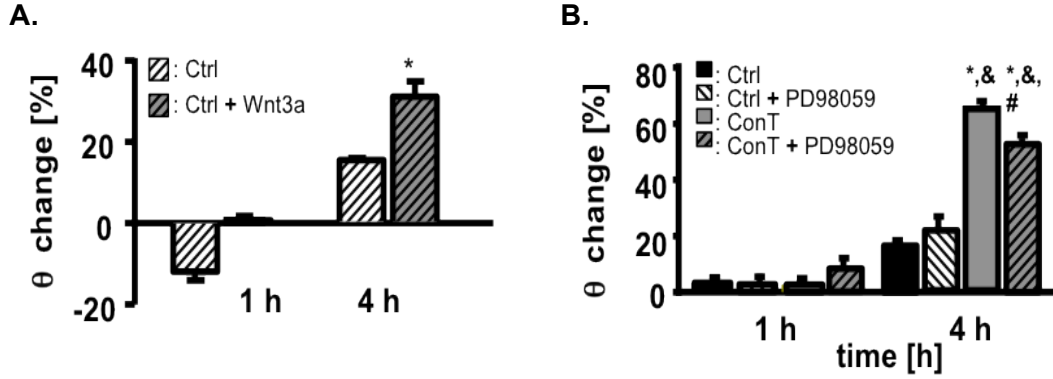


Figure 13: Canonical Wnt signaling and ERK1/2 signaling pathways affect Cx43 expression. Treatment of *HL-1* monolayers with media obtained from Wnt3a over-expressing L1 cells significantly increased the θ after 4h (A) (*: $p < 0.05$ compared to Ctrl). PD98058, an ERK1/2 inhibitor attenuated the ConT-mediated increase of θ in *HL-1* monolayers (B) (*: $p < 0.05$ compared to Ctrl; &: $p < 0.05$ compared to Ctrl+PD98059; #: $p < 0.05$ compared to ConT) [80].

4. DISCUSSION

We demonstrated that MSCs modulate the excitability and conduction of multicellular cardiomyocyte preparations by two different mechanisms. They can reduce spontaneous activity of cardiomyocyte monolayers by establishing intercellular coupling through gap junction channels; however, paracrine signaling can also increase the conduction velocity of the cardiomyocyte monolayer through upregulation of Cx43 without altering the beating frequency. An experimental examination supports an induction of Cx43 expression through the canonical Wnt/GSK3/ β -catenin signal transduction pathway in a Wnt and potentially ERK1/2 dependent and independent manner.

4.1 Influence of non-excitabile cells on cardiac excitation spread

Non-excitabile cells like fibroblasts and endothelial cells make up a significant portion of the ventricular muscle. Research has focused on the influence of these cells on the electrophysiological properties of the cardiac muscle. In vitro models demonstrate that electrotonic coupling of the non-excitabile cells can bridge excitation spread over spatially separated areas of myocytes [41, 89] and cause a decrease in θ in a dose (cell number) dependent manner [38, 79]. In co-cultures of MSCs and neonatal cardiomyocytes a >20% decrease in conduction velocity was reported in comparison to homocellular cardiomyocyte cultures and re-entrant arrhythmias could be more easily induced in the vicinity of MSCs clusters [47]. In our co-culture model, though there was a significant decrease in the spontaneous beat rate of *HL-1* cells as a consequence of the intercellular coupling, we did not observe a significant decrease of θ as previously described for *HL-1*/fibroblast co-cultures [38]. The lack of change in θ could be explained by the fact that the direct effect (capacitive coupling) of the MSCs is masked or compensated by the upregulation of Cx43 through paracrine signaling. However, since we were not yet able to isolate the effects induced by MSC/*HL-1*

intercellular coupling, other explanations have to be considered. Coupling of MSCs could be insufficient to induce changes in θ . Since we still see a decrease in beating frequency this would mean that θ is less sensitive to hetero-cellular coupling. This would still leave us to explain that no increase in θ was determined. The increase in θ could be prevented if *i.* the time of co-culture is insufficient to secrete enough active factors to induce Cx43 upregulation or *ii.* co-culture could change the MSC secretome. We could previously demonstrate, that MSC mediated increase in cardiomyocyte Akt phosphorylation was readily induced when co-culture was established and was unaffected from the presence of cardiomyocyte [61]. However, since Akt signaling does not play a role in Cx43 upregulation, we cannot rule out that changes in the secretome occur.

The paracrine effect of MSCs on θ described here was not previously examined however, in agreement with our data, MSCs have been shown to preserve impulse conduction [49], reduce the inducibility of ventricular arrhythmias [43] and improve atrioventricular conduction (AV) block [50]. The reason for the discrepancy in the co-culture models could be the result of the fact that in our cultures MSCs only comprised 10% of total cell number. This number is lower than the numbers that were previously tested in co-culture models [47]. In addition, in our co-culture model MSCs were added to an already established monolayer of cardiomyocytes and co-culture was monitored during the onset of hetero-cellular coupling. This is in contrast to other models where a mixture of MSCs and myocytes is plated [47]. Under these conditions MSCs spatially separate cardiomyocytes, which can increase the heterogeneity of the excitation wave-front. Our results would suggest that during integration of higher numbers of MSCs in a cardiomyocyte preparation the effect of the capacitive coupling could override the effect of the paracrine signaling on the conduction velocity; however, the previously established low retention of MSCs after transplantation suggests that paracrine signaling may play the predominate role to affect positive changes in the myocardium.

4.2 Influence of mesenchymal stem cells on HL-1 cell excitability and beating frequency

During co-culture of HL-1 cells and MSCs an attenuation of the spontaneous beating frequency was determined. This change in the rate of diastolic depolarization could be due to the direct effect of hetero-cellular coupling on the origin of excitation by depolarization of the *HL-1* cells or the increase in their capacitance. Alternatively, the coupling induced changes could result in a shift of the origin of excitation to an un-affected area or an area with increased pacemaker current. We have previously demonstrated that fibroblasts under the same conditions reduce spontaneous beating of *HL-1* monolayers through depolarization and increase of *HL-1* cell capacitance [38]. The fact that ConT alone had no impact on the spontaneous activity indicates that paracrine signaling induced no significant changes in *HL-1* excitability under the assumption that the secretome remained unchanged.

4.3 Mesenchymal stem cell mediated upregulation of connexin 43

In cardiomyocyte monolayers the major factors affecting θ are the cellular excitability, which is determined by the availability of Na channels and the intercellular resistance, which depends on the expression of gap junction channels. While we have previously described a ConT mediated increase in $I_{Ca,L}$ in adult ventricular myocytes [61], a change in cellular excitability is unlikely to fully explain the increase in θ determined in this study. The significant upregulation of Cx43 expression over the time period combined with no significant change in Na channel expression levels makes an increase in intercellular coupling the more likely explanation for the increase in θ . We also determined that ConT induced a moderate increase in the phosphorylation of Cx43. Overall the Cx43 phosphorylation levels in *HL-1* cells are low in comparison to the cardiac muscle where a decrease in Cx43 phosphorylation is often linked to pathophysiological remodeling [90]. Phosphorylation of Cx43 can regulate channel assembly,

electrical and metabolic coupling as well as trafficking. We can not rule out that the observed increase in phosphorylation of Cx43 changes the channels open probability or its turnover, however the change is relatively small to those previously described and likely only contributes slightly to the overall increase in θ .

4.4 Mesenchymal stem cell mediated paracrine signaling

MSCs secrete a broad spectrum of cytokines, chemokines and growth factors [40]. Some of these factors have been described to modulate intercellular coupling through Cx43. For VEGF, upregulation of Cx43 through the Raf-1 MAPK pathway has been reported [64] and for IGF-1 a PI3K/Akt and ERK mediated regulation of Cx43 was demonstrated [91]. Another signaling cascade involved in the regulation of Cx43 protein levels is induced by the secreted polypeptides of the Wnt family [65, 92]. In these cases upregulation of Cx43 is described through the Frizzled receptor via phosphorylation of GSK3- β and subsequent increase in β -catenin signaling [65]. Interestingly, our experimental results indicate that the PI3K/Akt pathway is not involved in the regulation of Cx43 expression although, we have previously demonstrated that it has a significant role in the ConT-mediated modulation of ECC in adult ventricular myocytes [61]. This result underlines the complexity of the signaling pathways induced by MSC conditioned media/tyrode. We used conditioned media as well as conditioned tyrode for our experiments. Since the composition of media is complex, we switched to tyrode to allow for a more controlled composition of the conditioned solution. The effect of ConM and ConT on θ and Cx43 expression was comparable therefore we decided to present the results together in this manuscript. However, we cannot rule out that the overall composition of ConM might vary from that of ConT but regarding the observed changes, both approaches had the same potency.

MSCs express Wnt proteins that are activators of the canonical (e.g. Wnt1, 2, 3, 8 and 8b) or non-canonical (Wnt4, 5a, 5b, 6, 7a and 11) pathway [83, 93]. They all play an important

role in the regulation of MSC proliferation and suppression of differentiation [94]. In our culture model Wnt-mediated signaling is supported by the ConT induced phosphorylation of LRP6, the fact that the increase in θ can partially be reproduced by Wnt3a conditioned media and by the sensitivity of the changes to pharmacological regulation of GSK3- α/β and β -catenin. Cardamonin reduced Cx43 expression levels and prevented changes in θ . In contrast to previous reports however, no significant changes in total β -catenin protein levels were determined [81]. This likely is explained by the slow turn-over time of β -catenin and our in comparison short cardamonin incubation time [95].

Suppression of Wnt formation by IWP-2 attenuated LRP6 phosphorylation and the increase of θ ; however, Cx43 protein levels at 4 h of treatment remained elevated in comparison to Ctrl. A potential explanation is that expression and degradation of Cx43 are both modulated by ConT. Even if Cx43 expression is suppressed, an increased stability of Cx43 in the gap junction plaques as it is proposed through Akt-dependent phosphorylation [96], could lead to an increase in θ . This would still be consistent with our experimental results that demonstrate no significant effect of Wortmannin on θ , since in that case expression of Cx43 would still be increased.

While we suppressed Wnt release from MSCs by IWP-2 treatment, we were not able to completely suppress ConT mediated LRP6 phosphorylation. Besides the binding of Wnt agonists, phosphorylation of LRP6 has been described through receptor tyrosine kinases (RTK) mediated ERK activation in a PI3K/Akt independent manner [87]. The LRP6 activation then could still induce β -catenin signaling and subsequently an increase in Cx43 expression. A partial involvement of *p*-ERK1/2 in Cx43 upregulation is supported by our experiments (Fig. 8B).

Ischemia reperfusion injury as well as cardiac hypertrophic growth are often related to decreased levels of Cx43 expression, which itself is linked to an increased propensity in cardiac arrhythmia [97]. A Wnt-mediated upregulation of Cx43 could therefore promote anti-arrhythmic

activity as it was described in a transgenic cardiomyopathic mouse model [65]. It has to be mentioned that the enhanced cardio-protective effect of Akt over-expressing MSCs was linked to their increased secretion of Sfrp [60, 98]. Sfrp suppresses Wnt signaling which under pathophysiological conditions suppresses Wnt induced apoptosis [98]. Additionally it is proposed that the suppression of Wnt promotes stem cell differentiation thereby enhancing cell replacement and vascularization [59, 60, 99]. If the Wnt dependent upregulation of Cx43 or the suppression of Wnt signaling through Sfrp represent the mechanism of cardioprotection during transplantation of MSCs will likely depend on the physiological or pathophysiological phenotype of the cardiac tissue.

5. CONCLUSION

We demonstrated that MSCs rapidly establish intercellular coupling with cardiac myocytes. While the added capacitance of the MSCs decreases the excitability of the myocytes, a reduction in the conduction velocity of excitation spread is prevented by upregulation of Cx43 protein levels. Changes in Cx43 expression are induced through paracrine signaling of MSCs involving the stimulation of the canonical Wnt signaling pathway. Consequently, during pathophysiological remodeling transplantation of MSCs or treatment with MSC conditioned medium could help maintain coordinated excitation spread by promoting Cx43 expression. Figure 14 shows a summary schematic of the signal transduction pathway involved in upregulation of Cx43 resulting in an increased cardiac conduction.

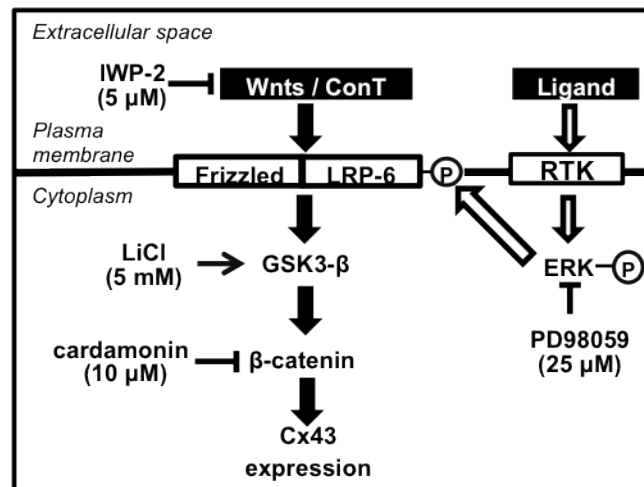


Figure 14: A schematic summary of the experimental results illustrates the proposed signal transduction pathway [80].

CHAPTER 2

1.INTRODUCTION

1.1 Transverse-tubule network

Transverse-tubules (T-tubules) are subcellular structures that are formed by the invaginations of the sarcolemma and occur at the Z-line in mammalian ventricular myocytes. They provide close structural proximity between the excitable cell membrane and the sarcoplasmic reticulum (SR), which is the main intracellular Ca^{2+} store in the myocyte. T-tubules of the myocyte have a mean diameter of 200-300 nm and occur at $\sim 2 \mu\text{m}$ intervals near the Z-lines [100]. Figure 15 shows a simplified schematic representation of the uniform t-tubular system and the organization of the protein machinery that cause excitation-contraction coupling in an adult mammalian ventricular myocyte.

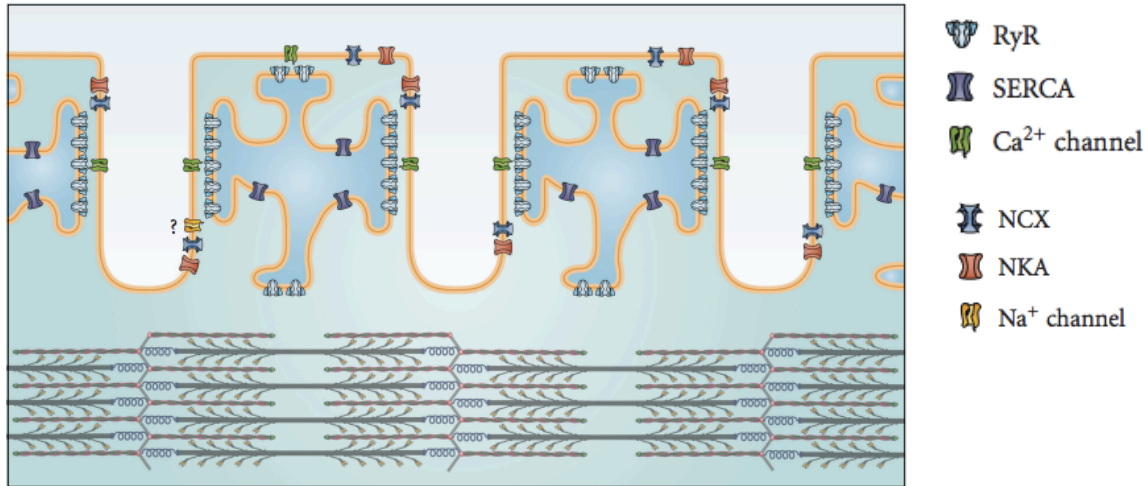


Figure 15: Schematic representation of the t-tubular system and the neighboring protein machinery. Excitation-contraction coupling occurs at functional junctions between Ca^{2+} channels in the t-tubules and ryanodine receptors (RyR) in the SR. Depending on their localization, other proteins such as SR Ca^{2+} ATPase (SERCA), Na-Ca exchanger (NCX), Na^+/K^+ -ATPase (NKA), and Na^+ channels can also regulate Ca^{2+} homeostasis (Obtained with permission and modified from [101]).

T-tubules occur in cardiomyocytes of mammals such as mice [102], rats [103], rabbits [104], pigs [105], dogs [106] and humans [107]. They are predominantly found in ventricular myocytes and less abundant in tissue of the pacemaker or the conduction system [108]. Recent studies have confirmed a t-tubular system in atrial myocytes belonging to rat [109], sheep [110], cow, horse and humans [111]. The central point of t-tubular function is to extend the voltage dependent Ca^{2+} influx into the depth of the cell [112]. As described by Bers DM [20], contraction in cardiomyocytes is initiated by depolarization-mediated Ca^{2+} entry via the L-type Ca^{2+} channels resulting in triggered Ca^{2+} release from the SR via the ryanodine receptor 2 (RyR2).

This t-tubule mediated close spatial interaction of the sarcolemmal L-type Ca^{2+} channels and the RyR2 allows for the rapid and homogeneous release of Ca^{2+} throughout the cell via the calcium-induced calcium release (CICR) action. Thus the t-tubule structure determines the homogeneity of the CICR occurring in the myocyte during depolarization. Therefore, it is vital to understand the mechanisms involved in the development, regulation and maintenance of the t-tubular system under both physiological and pathophysiological conditions.

1.2 Transverse-tubule regulation and remodeling

As indicated, the t-tubular system plays a functional role in promoting the rapid and homogeneous release of Ca^{2+} from the SR throughout the cell during systole. It has been observed that under pathological conditions, t-tubules undergo remodeling [113]. This t-tubule remodeling disrupts the close spatial interaction of the L-type Ca^{2+} channels and the RyR2 leading to voltage dependent Ca^{2+} entry only at the cell periphery. Consequently, the Ca^{2+} release at the center of the cell under these conditions depends on Ca^{2+} diffusion, amplified by Ca release from RyRs leading to a delayed Ca release in the center of the cell. This altered CICR results in a prolongation of the Ca^{2+} transient rise time and therefore an attenuation of the Ca transient amplitude, which ultimately causes decreased contractility of the myocardium [114].

While the disease associated t-tubular remodeling is well documented, little is known about the mechanism of t-tubular formation and maintenance. Two proteins have recently been attributed prominent roles in t-tubule formation [115]. Amphiphysin 2, or alternatively called myc box-dependent-interacting protein 1 (BIN1) was shown to promote the formation of t-tubular structures. When BIN1 is expressed in non-muscle cells, it induces the formation of invaginations of the plasma membrane resembling t-tubule morphology [116]. *In vivo* disruption of BIN1 in murine embryos resulted in malformed t-tubular system, embryonic cardiomyopathy

and perinatal lethality [117]. BIN1 was further described to shuttle L-type calcium ($\text{Ca}_v1.2$) channels to the t-tubules in cardiac muscle [118] thereby not only regulating the t-tubular structure but also maintaining its function. Junctophilin 2 has been described to regulate the junction formation between the SR and t-tubules. Its downregulation correlates with the hearts transition from hypertrophy to HF which is associated with the impaired CICR due to the uncoupling of SR and t-tubules [119] [120]. Pathological remodeling of t-tubules can be caused by myocardial insults such as sustained tachycardia [121], myocardial infarction [122] and spontaneous hypertension [123] leading to disorganization and loss of the uniform t-tubular system. Recent experimental data indicate that t-tubule changes occur early in the transition from hypertrophy to HF and could be a potential early pathogenic mechanism that further enhances cardiac remodeling [120] [124].

In recent years, elevated levels of reactive oxygen species (ROS) causing oxidative stress have been implicated as an underlying mechanism for cardiac remodeling during pathological conditions such as hypertrophy [125] and heart failure [126]. It has been reported that increased ROS production stimulates cardiac fibroblast proliferation [127], activation of matrix metalloproteinases (MMPs), effects central to fibrosis and matrix remodeling [128] [129]. ROS was further shown to modify proteins central to excitation-contraction coupling such as RyR, L-type Ca channels and SERCA. By modification of thiol groups (-SH) ROS enhances the open probability of RyRs [130], decreases SERCA activity and suppresses $I_{\text{Ca,L}}$ leading to an overall decrease in Ca transient amplitude and delayed recovery [131]. Intracellular ROS can be generated via four pathways in the cardiomyocytes namely: through activation of nicotinamide-adenine dinucleotide phosphate (NADPH) oxidase (NOX) or xanthine oxidase (XO), uncoupling of nitrous oxide synthase (NOS), and electron transport during oxidative phosphorylation in the mitochondria [132]. Among the five isoforms of NOX, NOX2 and NOX4 are predominantly found in the myocardium [125]. During the development of pressure-overload hypertrophy in guinea

pigs [133] and human heart failure [134] as well as in angiotensin II-induced cardiac hypertrophy/remodeling an increased NOX activity and expression has been observed that plays a critical role in remodeling [135]. An exacerbating factor is that NOX-mediated ROS production can further induce NOS3 uncoupling [136] and activate XO [137] thereby enhancing ROS production. Recent evidence from a mouse model that lacks the expression of the p21-activated kinase shows that increased NOX2 dependent ROS production in cardiomyocytes correlates with decreased t-tubular density [138] without any further indications of cardiac hypertrophic remodeling. These data would implicate for the first time ROS as a potential initiator of t-tubular remodeling.

The basic underlying mechanisms responsible for t-tubule dysregulation are still unknown. Most studies that address t-tubular dysregulation were obtained under cell culture conditions, taking advantage of the fact that ventricular myocytes lose their t-tubular system after cell isolation in a time dependent manner [113]. Results from these studies indicate that t-tubule loss is enhanced when cells are maintained at rest and that actin remodeling is a contributing factor to the loss of the t-tubular system [139] [140].

Based on the observations described above we will use the in-vitro model of t-tubular remodeling to test the hypothesis that NOX-mediated ROS production plays a role in t-tubular remodeling. The primary aim of the study is to determine the role of ROS generated in the cardiomyocytes in t-tubule remodeling and elucidate molecular targets that could potentially reverse the ROS-induced t-tubule remodeling *in vitro*.

2. MATERIALS AND METHODS

2.1 Cell isolation and culture

Isolated adult rabbit ventricular myocytes (VMs) were obtained from Dr. Blatter's laboratory at Rush University where isolation protocols were followed as previously described [141] [142]. Cells were plated on laminin (1mg/ml) coated sterilized glass coverslips (18 mm diameter) and cultured in either 6 well or 12 well tissue culture plates in DMEM (1X) + GlutaMAX (Gibco, Invitrogen) supplemented with creatine (2 mmol/L; Sigma Aldrich), carnitine (2 mmol/L; Sigma Aldrich), taurine (5 mmol/L; Sigma Aldrich), penicillin streptomycin (Pen Strep) (15,000 units/ml; Gibco Life Technologies) and non-essential amino acids (100x; Gibco Life Technologies) [143]. The cells were treated with the antibiotic, gentamicin (1 µg/L/ml; Invitrogen) for 1 h during cell plating in order to address contaminating microbial growth introduced into the culture during the isolation protocol. Rabbit ventricular myocytes were maintained in culture for up to 48 h.

Cell plating on pre-coated laminin coverslips was carried out as described in the literature [144]. Glass coverslips were ethanol and flame sterilized. After sterilization, 4 µl of laminin was spread on the coverslip evenly over a circular area covering approximately 70% of the coverslip. Coverslips were then placed into either a 12-well or 6-well tissue culture plate and dried before plating the cells. Dispersed rabbit VMs were added directly to each coverslip in a 200 µl volume and allowed to adhere for 8 min prior to addition of medium. The coverslips were held undisturbed for 20 min at room temperature and then moved to the tissue culture incubator. 1 h after plating, dead cells were aspirated along with media and 2 ml of fresh media was added to each well. Pharmacological treatment of the cells was carried out after the change of the media and the cells were examined after 24 h and 48 h. Control groups were cultured alongside for the same period of time.

2.2 Pharmacological treatment of rabbit ventricular myocytes

Tempol (100 $\mu\text{mol/L}$; Calbiochem), a ROS scavenger was used to treat the rabbit VMs for 48 h [145]. A stock solution of 100 mmol/L was prepared by dissolving 52 mg of Tempol in 3 ml of dimethyl sulphoxide (DMSO). 2 μL of this 100 mmol/L Tempol stock solution was added to each well to achieve a final concentration of 100 $\mu\text{mol/L}$. The scavenger was replenished in culture every 24 h.

Apocynin (200 $\mu\text{mol/L}$; Sigma Aldrich), a NADPH oxidase inhibitor was used to treat the rabbit VMs for 48 h [146]. A stock solution of 25 mmol/L was first prepared by dissolving 8.3 mg of Apocynin in 2 ml of dimethyl sulphoxide (DMSO). To each well having a volume of 2 ml media, 16 μL of the 25 mmol/L stock solution of Apocynin was added to achieve a final concentration of 200 $\mu\text{mol/L}$. The inhibitor was replenished in culture every 24h to maintain the final concentration in culture.

Mito-TEMPO (10 $\mu\text{mol/L}$; Enzo Life Sciences), a mitochondrial-ROS scavenger was used to treat the rabbit VMs for 48 h [147]. To each well having a final volume of 2 ml media, 4 μL of the 10 mmol/L stock solution of Mito-TEMPO was added to achieve a final concentration of 5 $\mu\text{mol/L}$. The scavenger was replenished in culture every 24h to maintain the final concentration in culture.

2.3 Field stimulation of rabbit ventricular myocytes

It has been demonstrated that t-tubular remodeling is accelerated when the cells are maintained under non-stimulated conditions [113, 139]. Therefore control as well as pharmacologically treated rabbit VMs was maintained in culture while they were paced using a C-100 Pace EP cells culture stimulator (IonOptix Corporation). Cells were paced for a period of 48h at 0.5 Hz frequency for a duration of 4 ms with a voltage strength of 20 V. Cells were evaluated after 24 h and 48 h with di-8-ANEPPS staining for t-tubule imaging.

2.4 Transverse-tubule imaging

To evaluate the T-tubule network density in rabbit VMs after 24 h and 48 h in culture using confocal imaging, the cells were transferred to Kraft Bruhe solution (KB; 5 mmol/L Hepes, 5 mmol/L MgSO₄, 10 mmol/L glucose, 90 mmol/L KCl, 30 mmol/L K₂HPO₄, 5 mmol/L sodium pyruvate, 1.09 mmol/L NaOH, 0.5 mmol/L EGTA, 20mmol/L taurine, 5 mmol/L creatine and 5 mmol/L NaCl, pH 7.3). These depolarizing and zero-Ca condition guarantees the relaxation of the VM and prevents potential movement artifacts. To stain the sarcolemmal membranes, the cells were loaded with di-8-ANEPPS (7.5 µmol/L; Life Technologies) for 20 min prior to the start of image acquisition. This dye is weakly fluorescent in aqueous media, but become strongly fluorescent upon binding to lipophilic environments such as membranes. Z-stack images were taken using a krypton (Kr) laser exciting at 488 nm and a 60-X water immersion objective lens at 50 lines per sec (lps) scan rate. Each optical section was imaged at 1 µm interval.

2.5 Image analysis

Image analysis was carried out using two different methods. The first method involved the computation of percentage area occupied by the positively stained t-tubules in a user defined selection area within a cell using Image J (National Institutes of Health, Bethesda, MD). The confocal optical sections were converted to binary images and an area within the cell was outlined excluding the plasma membrane and the nucleus. The percentage area occupied by di-8-ANEPPS stained t-tubules was then determined and averaged for each cell by considering six consecutive z-stack confocal images. As a second method, power spectral analysis of the t-tubular system using two-dimensional Fast Fourier Transform (FFT) analysis was computed using IGOR Pro 6.0 (WaveMetrics Inc., Portland, OR). Line profiles (width = 5 pixels) for three equivalent Z-stack images for each cell were generated in Image J. The pixel intensity data for each line profile was imported into the software for analysis. The real component (power) was

plotted against the spatial frequency and represented as the power spectrum after performing FFT. The power spectra were normalized to the baseline low frequency to the right of the characteristic peak occurring between $0.5 \mu\text{m}^{-1}$ - $0.6 \mu\text{m}^{-1}$ indicating the repetition of t-tubule structures at $2 \mu\text{m}$ intervals [139] [148]. Figure 16 (A, B, C) depicts a schematic representation of the steps involved in di-8-ANEPPS stained t-tubule image analysis using FFT.

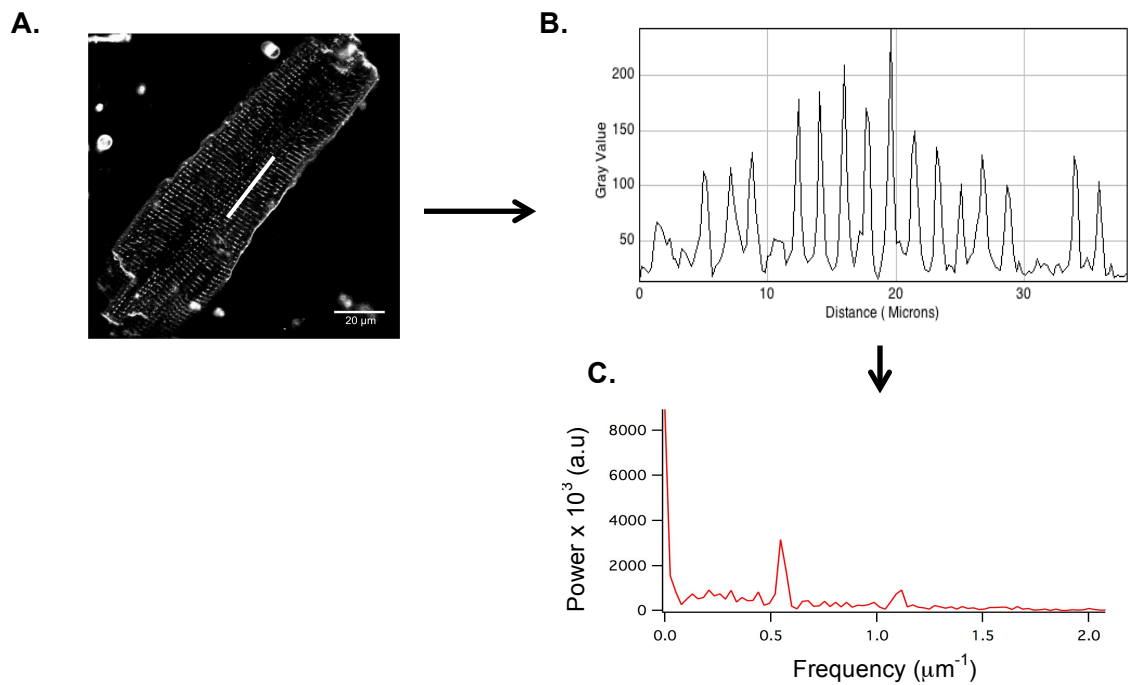


Figure 16: Schematic representation of the major steps involved in image analysis using fast fourier transform (FFT) technique. A confocal image of di-8-ANEPPS stained t-tubules of an isolated ventricular myocyte (A). Line intensity profile generated along the white line shown in

(A) using Image J (B). Resultant power spectra obtained after FFT using the line intensity profile in IGOR Pro (C).

2.6 Statistical analysis

Experimental values were compared to controls using an unpaired two-tailed Student's t-test statistics. Data are presented as mean \pm SEM. Differences were considered significant at $p < 0.05$.

3. RESULTS

3.1 Inhibition of nicotinamide adenine dinucleotide phosphate-oxidase-dependent reactive oxygen species production modulates transverse-tubule network

To test the hypothesis that t-tubular remodeling is mediated by increased ROS production via NOX, freshly isolated rabbit VMs were treated with Apocynin, a NOX inhibitor and compared with untreated Control cells. Cells positively stained with di-8-ANEPPS were imaged using confocal microscopy. Representative confocal images of di-8-ANEPPS stained t-tubules (Fig. 17 A, B) qualitatively demonstrate that Apocynin treated cells exhibit a conserved t-tubular system after 24 h compared to untreated Controls. This is further quantitated and shown below in the corresponding power spectrum displaying the characteristic peak of t-tubule occurrence at $0.5\ \mu\text{m}^{-1} - 0.6\ \mu\text{m}^{-1}$ (Fig. 17 C) in Control and Apocynin treated VM after 24 h in culture.

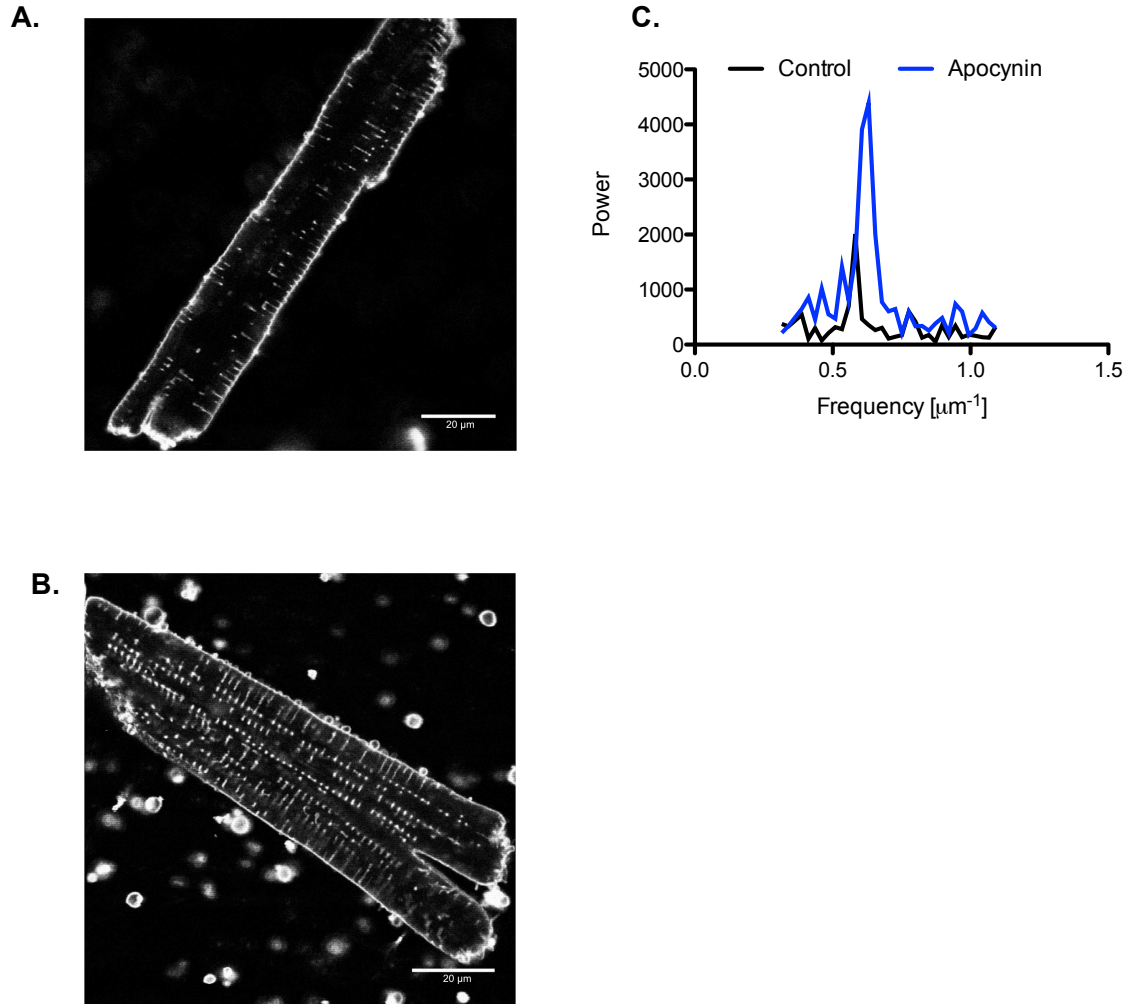


Figure 17: Confocal image of di-8-ANEPPS stained t-tubules and the corresponding power spectrum depicting t-tubular density. Representative images of the di-8-ANEPPS stained t-tubule network in rabbit ventricular myocyte after 24 h from both Control (A) and Apocynin treated groups (B) and the corresponding power spectrum showing the characteristic peak occurrence ($0.5 \mu\text{m}^{-1} - 0.6 \mu\text{m}^{-1}$) indicating t-tubule network existence in Control and Apocynin treated VMs after 24 h (C).

In accordance to studies demonstrating a progressive loss of t-tubules *in vitro* [139, 140] [113], our culture model too showed t-tubular remodeling in a time dependent manner. Rabbit VMs exhibited t-tubular loss in culture for 48 h (Control: t-tubule_{0h}: 4.99 ± 0.60 , n = 20; t-tubule_{24h}: 2.99 ± 0.38 , n = 14; t-tubule_{48h}: 3.22 ± 0.56 , n = 16) (Fig. 18A). Treatment with Apocynin attenuated this rate of t-tubular loss in culture significantly when compared to untreated control cells after 24 h (Apocynin: t-tubule_{24h}: 4.69 ± 0.70 , n = 15, p < 0.05; Control: t-tubule_{24h}: 2.99 ± 0.38 , n = 14). However, no significant change in rate of t-tubular loss was observed between Apocynin treated and untreated VMs following 48 h (Apocynin: t-tubule_{48h}: 2.905 ± 0.42 , n = 17; Control: t-tubule_{48h}: 3.22 ± 0.56 , n = 14) (Fig 18A). Analysis of the above experimental data as a percentage of area occupied by the di-8-ANEPPS stained t-tubules normalized to the control cells revealed the same result at 24 h (Apocynin: t-tubule_{24h}: 0.718 ± 0.138 , n = 15, p < 0.05; Control: t-tubule_{24h}: 0.274 ± 0.062 , n = 14) and at 48 h (Apocynin: t-tubule_{48h}: 0.194 ± 0.04 ; n = 17; Control: t-tubule_{48h}: 0.282 ± 0.06 , n = 14) (Fig. 18B).

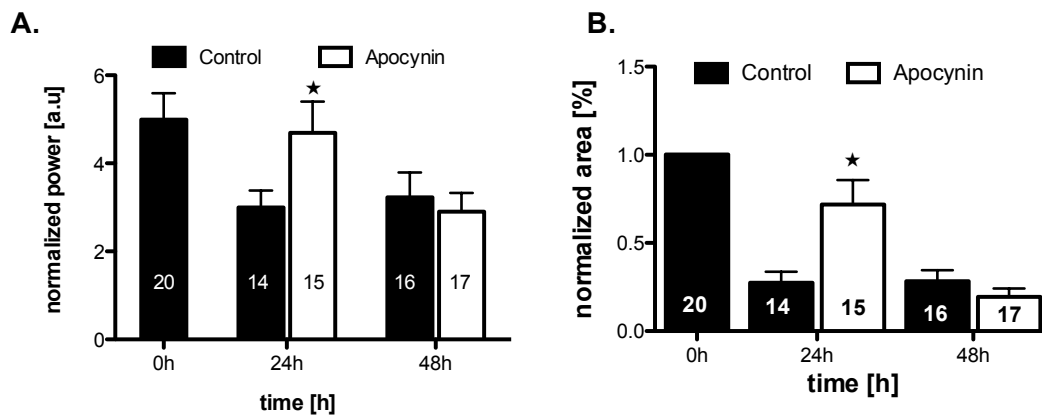


Figure 18: Inhibition of NOX dependent ROS production modulates the rate of t-tubular loss. T-tubule density in isolated rabbit ventricular myocytes in Control and Apocynin treated cells as a function of time (A). T-tubule density in Control and Apocynin groups represented as percent area normalized to controls at 0 h (B) (*: $p < 0.05$ compared to Control) [Number in the bars represent the number of cells analyzed in each group].

This transient effect of Apocynin only in the early phase (24 h) could indicate that t-tubular remodeling occurs via a NOX dependent mechanism. However, no effect of the NOX inhibitor in the late phase (48 h) may dictate the role for a secondary mechanism contributing to t-tubular remodeling. It has been previously demonstrated that lack of contractile activity due to resting can accelerate t-tubular remodeling *in vitro* and electrical stimulation/pacing could attenuate this remodeling and improve contractile properties [149]. To distinguish if the enhancement in t-tubular remodeling was due to lack of contractile activity or increased ROS production via NOX in our culture model, the experiment involving NOX inhibition using Apocynin was repeated in rabbit VMs that were field stimulated during their time in culture. Percentage of t-tubules preserved in Control cultures under non-paced and paced conditions

was plotted as a function of time (Fig. 19A, B) to evaluate the effect of electrical stimulation in attenuating rate of t-tubular loss. It was observed that pacing (Control: t-tubule_{24h}: 61.8 % \pm 10.23, t-tubule_{48h}: 30.5 % \pm 0.659) (Fig. 19B) did not significantly enhance the preservation of t-tubular system in control cultures when compared to non-paced control cultures (Control: t-tubule_{24h}: 60.4 % \pm 3.79, t-tubule_{48h}: 64.5 % \pm 12.07). However on further observation, the rabbit VMs used for the pacing experiments (Day1: 8.38 \pm 1.00, n = 9 cells; Day 2: 9.17 \pm 0.56, n = 11 cells; Day 3: 6.75 \pm 1.16, n = 10) showed a higher t-tubule density to begin with on the day of isolation compared to the cells used for the non-paced experiments (Day1: 5.84 \pm 1.06, n = 9 cells; Day 2: 4.28 \pm 0.63, n = 11 cells) (Fig. 19C, D). These data indicate an inherent variability in the t-tubular densities occurring in these cells shortly after isolation. Treatment of paced VMs with Apocynin significantly attenuated the rate of t-tubular loss in comparison to Control cells at both 24 h (Apocynin: t-tubule_{24h}: 6.90 \pm 0.71, n = 30, p < 0.05; Control: t-tubule_{24h}: 4.94 \pm 0.48; n = 27) and at 48 h (Apocynin: t-tubule_{48h}: 4.62 \pm 0.79, n = 21, p < 0.05; Control: t-tubule_{48h}: 2.52 \pm 0.50; n = 22) (Fig. 19E). These results suggest that NOX-dependent ROS generation could play a potential role in t-tubular remodeling.

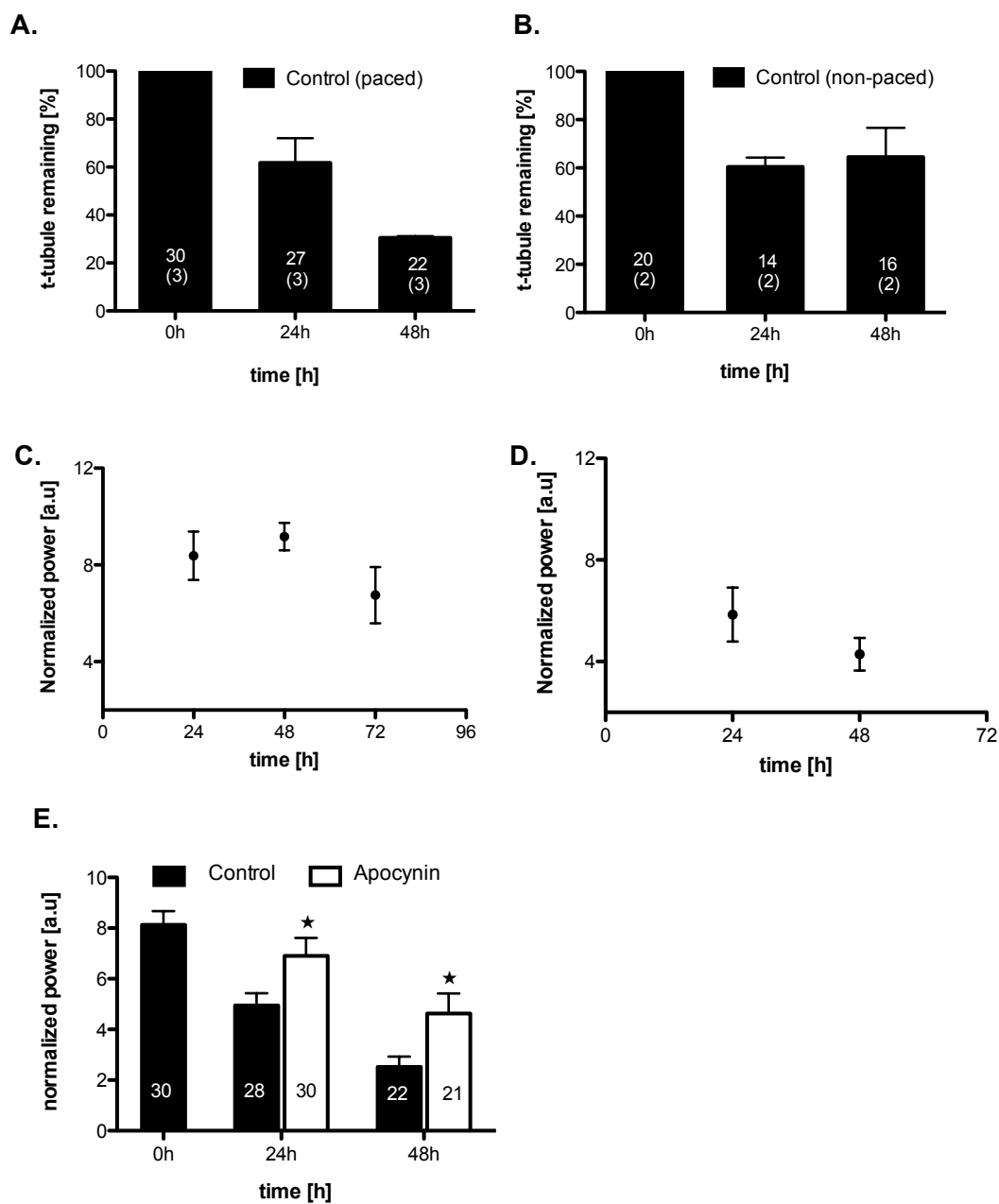


Figure 19: Integrity of t-tubular system in paced and non-paced conditions. Percentage of t-tubules preserved in control cultures as a function of time in paced (A) and non-paced conditions (B). T-tubule density of cells used for paced (C) and non-paced experiments (D) following isolation during different experimental days. The rate of t-tubular loss as a function

of time in Control and Apocynin treated groups (E) [Number in the bars represent the number of cells analyzed in each group and number within the parenthesis indicate number of animals from which the cells were obtained].

3.2 Effect of mitochondrial and cytoplasmic reactive oxygen species and transverse-tubule remodeling

Apocynin treatment did not entirely prevent t-tubular loss *in vitro* and hence we aimed to determine if alternative sources of ROS contributes to t-tubular remodeling. For this purpose, non-paced VMs were treated with a mitochondrial and cytoplasmic ROS scavenger, Mito-TEMPO and Tempol respectively, for 48 h. Tempol and Mito-TEMPO treatment did not significantly attenuate the rate of t-tubular loss as compared to untreated controls at 24 h (Tempol: t-tubule_{24h}: 5.22 ± 0.72 , n = 18; Mito-TEMPO: t-tubule_{24h}: 4.33 ± 0.58 , n = 17; Control: t-tubule_{24h}: 5.03 ± 0.74 , n = 19) and at 48 h (Tempol: t-tubule_{48h}: 3.51 ± 0.43 , n = 18; Mito-TEMPO: t-tubule_{48h}: 2.98 ± 0.49 , n = 17; Control: t-tubule_{48h}: 3.49 ± 0.71 , n = 16) (Fig. 20A). The overlay of representative power spectra depicting t-tubular density in control and treatment groups indicates the characteristic peak occurrence of t-tubules at $0.5 \mu\text{m}^{-1}$ after 48 h (Fig. 20B). Analysis of the above experimental data as a percentage of area occupied by di-8-ANEPPS stained t-tubules normalized to the control cells also revealed the same result following 48 h (Tempol: t-tubule_{48h}: 0.293 ± 0.03 , n = 18; Mito-TEMPO: t-tubule_{48h}: 0.228 ± 0.03 , n = 17; Control: t-tubule_{48h}: 0.365 ± 0.05 , n = 16) (Fig. 20C). These results suggest that scavenging of mitochondrial and cytoplasmic ROS does not significantly contribute to attenuating rate of t-tubular loss in culture.

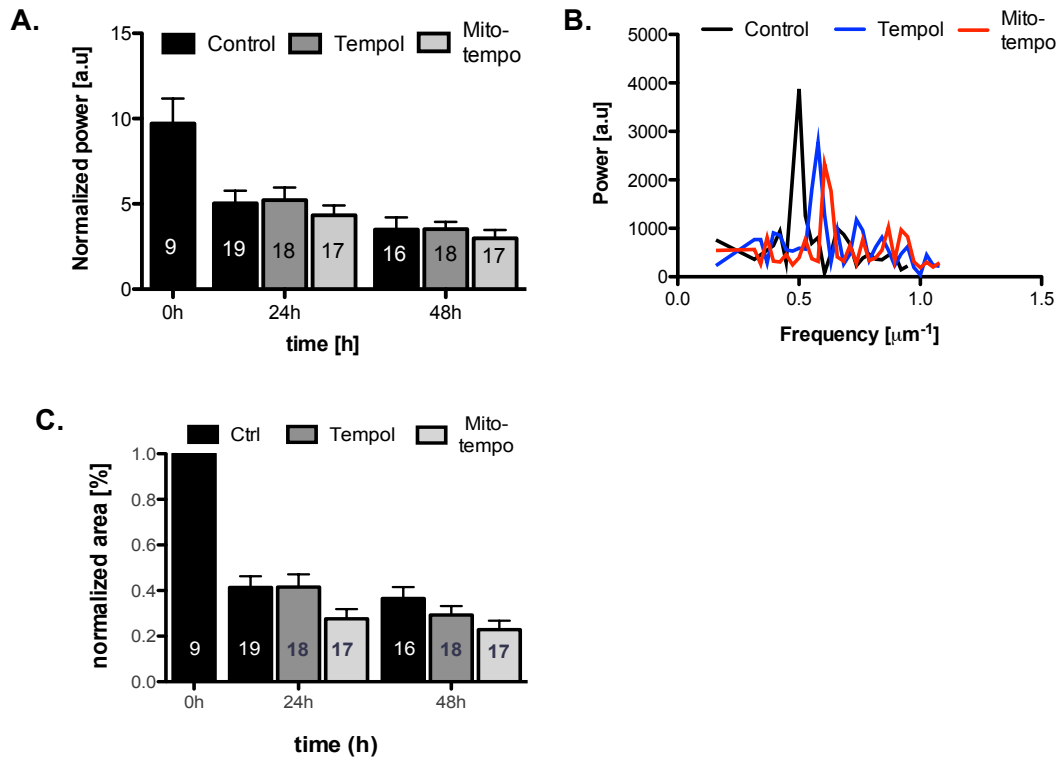


Figure 20: Inhibition of cytoplasmic and mitochondrial-ROS production does not reduce the rate of t-tubule loss in non-paced VMs. T-tubule density analysis using FFT of isolated rabbit ventricular myocytes after Control, Tempol and Mito-TEMPO treatment for 48 h in non-paced cultures (A) (n = 2 animals) [Number on the bars represent the number of cells analyzed in each group]. Power spectrum showing the characteristic peak occurrence ($0.5 \mu\text{m}^{-1}$ - $0.6 \mu\text{m}^{-1}$) indicating t-tubule network integrity in Control, Tempol and Mito-TEMPO groups after 48 h (B) and t-tubule density represented as normalized percent area (C).

4. DISCUSSION

This study demonstrates a putative role for NOX-mediated ROS production in t-tubular remodeling in culture. Treatment of rabbit VMs with a NOX inhibitor significantly attenuated the rate of loss of t-tubules in culture. However, results using global and mitochondrial ROS scavengers remained inconclusive. Overall the results could suggest that NOX dependent ROS regulates t-tubular remodeling in our culture model but the experimental results need to be verified by the use of additional NOX2 inhibitors and ROS scavengers. At this point no conclusions can be drawn by which mechanism ROS influences t-tubules or their regulating proteins.

T-tubule integrity was analyzed using two image analysis techniques as described in the method sections. The first method involves generating binary images based on the input image, which could either be in gray scale or color. Binary images contain only black and white pixels and an intensity threshold value determines assigning each intensity in the input image to either black (background) or white (foreground). This therefore enables the separation of the areas of interest in the image as foreground from the areas that belong to the background. This kind of image processing is known as thresholding of images [150] and was implemented in this study using Image J. Determination of the intensity threshold value is carried out with respect to the user-defined selection area by the default *isodata* thresholding algorithm in ImageJ and this strategy can introduce an intrinsic variability of user-defined bias in computing the t-tubule density. Additionally, one can choose from different algorithms to threshold images, which can further enhance the variability in the analysis. Therefore, a second technique was used which involved employing FFT technique to process images. This analysis determined the frequency of occurrence of a repeating element in an image. The default algorithm used by Igor Pro to carry out FFT is Cooley-Tukey algorithm [151]. Results obtained from both image-processing techniques were comparable, indicating that the user-defined bias introduced by the

thresholding technique does not influence in the experimental conclusions. Nevertheless, the FFT technique was adopted for image analysis in this study.

In contrary to experimental results obtained by Tomori K et al [149], rate of t-tubular loss due to contractile inactivity was not significantly attenuated by electrical stimulation in our culture model. One reason for this discrepancy could be that the VMs used for the study started out with an attenuated t-tubular density, immediately after isolation from the animal. (Fig. 19 C, D). This could be due to variations in isolation quality or inherent variability in t-tubule structures among the rabbits even before cell isolation. To address this problem replicate experiments need to be carried out with cells isolated from more animals for the non-paced cultures and paced cultures.

Mechanisms underlying t-tubular remodeling are still incompletely understood. NOX-mediated ROS production has been shown to cause pathological remodeling of cardiac tissue [152]. A significant and sustained increase in NADPH oxidase activation was found that correlated with increased expression of NOX2, p22 *phox* and p67 *phox*, in cardiomyocytes of a guinea-pig model of pressure overload left ventricular hypertrophy (LVH) [133]. Additionally, NOX2-deficient mice subjected to aortic banding showed evidence of significantly better contractile function than wild-type animals both in whole hearts and at the level of isolated cardiomyocytes thereby suggesting that increased ROS, has a direct effect on contractile function [153]. NOX2 and its associated oxidase subunit expression have shown to be increased at sites of infarcted myocardium in a rat model [65].

In vitro experiments examining the role of the cytoskeletal remodeling in t-tubular maintenance have shown that actin stabilization significantly attenuated t-tubular remodeling [140, 148]. Experiments in non-cardiomyocytes demonstrated that H₂O₂ as well as Angiotensin II treatment leads to ROS dependent actin rearrangement [154]. However, at this point we can only speculate that the ROS dependent modulation of actin filaments contributes to t-tubular remodeling in culture.

An interesting finding of these preliminary experiments is that in contrast to the NOX inhibitor, treatment of VMs with either Tempol or Mito-TEMPO did not affect t-tubular remodeling. The lack of effect of Mito-TEMPO could indicate that mitochondrial oxidative stress may not contribute to the remodeling process; however, we had hypothesized that the cytoplasmic ROS scavenger to mimic the effect of Apocynin. One reason for this could be that the effects on t-tubular remodeling by Apocynin dependent NOX inhibition are different from scavenging the produced ROS. This could be determined by the use of other NOX or NOX2 specific inhibitors or analysis of t-tubular remodeling in NOX2 knockout (NOX2 KO) mice. Alternatively it could be that inhibition of ROS production in comparison to scavenging the already produced ROS more effectively attenuates t-tubular remodeling. Yet another explanation could be that the concentration of Tempol used in this study (100 $\mu\text{mol/L}$) was ineffective in scavenging all the cytoplasmic ROS. Use of higher concentrations of Tempol (ranging from 0.5 mmol/L - 1 mmol/L) has been shown *in vitro* studies [155]. Therefore, further experiments need to be conducted to investigate the causal roles played by ROS produced in the cell in t-tubule remodeling. Although, the results suggest that NOX-dependent ROS generation could potentially enhance t-tubular remodeling *in vitro*, remodeling of the t-tubular system could not be completely prevented by inhibition of this pathway. Hence, ROS produced from alternative sources or secondary mechanism such as lack of contractile activity cannot yet be ruled out as a significant contributor to t-tubular remodeling. Further experiments need to be conducted to elucidate the underlying mechanism initiating t-tubular remodeling.

5. CONCLUSION

Inhibition of NOX-mediated ROS production by Apocynin attenuates but does not prevent the rate of t-tubular loss in rabbit VMs under both paced and non-paced conditions indicating that NOX-dependent ROS generation may play a potential role in t-tubular remodeling. While further experiments are necessary to clarify the role and the source of ROS that influences t-tubular remodeling, these initial experiments indicate ROS as a pharmacological target to attenuate subcellular remodeling during hypertrophy and the consequent decrease in contractile function.

6. FUTURE DIRECTIONS

The preliminary experiments presented here served to address the specific aim of the study, which is, to investigate the relationship between ROS production and t-tubule remodeling. Further experiments need to be conducted so as to address the discussed concerns of the preliminary data obtained. To clarify whether pacing of the VMs contributes to prolonged maintenance of t-tubules in culture, replicate experiments need to be carried out for both paced and non-paced culture conditions. Treatment of rabbit VMs with higher concentrations of Tempol need to be conducted to eliminate a concentration dependent effect on its efficacy to scavenge cytoplasmic ROS. Alternatively, treatment of VMs with inhibitors to block the two predominant isoforms, NOX2 and NOX4 in cardiomyocytes need to be carried out. To strongly implicate that NOX dependent ROS produced is a potential contributor to t-tubular remodeling, experiments need to be carried out using cells from NOX KO animals in addition to studies conducted using NOX2/NOX4 inhibitors. Measurement of ROS levels produced in both control and Apocynin treated cells have to be carried out to determine the possible direct role played by ROS in t-tubular remodeling. Future experiments will also involve the measurement of ROS-dependent modification of the proteins regulating the cytoskeletal elements such as actin.

CITED LITERATURE

- [1] World Health Organization. 2011.
- [2] Ranganath SH, Levy O, Inamdar MS, Karp JM. Harnessing the mesenchymal stem cell secretome for the treatment of cardiovascular disease. *Cell stem cell*. 2012;10:244-58.
- [3] Cardiovascular Regenerative Medicine: The Developing Heart Meets Adult Heart Repair. *Circulation Research*. 2009;105:1041-3.
- [4] Cohn JN, Ferrari R, Sharpe N.- 35:- 582.
- [5] Gaudron P, Eilles C, Kugler I, Ertl G. Progressive left ventricular dysfunction and remodeling after myocardial infarction. Potential mechanisms and early predictors. *Circulation*. 1993;87:755-63.
- [6] Anversa P, Olivetti G, Capasso JM. Cellular basis of ventricular remodeling after myocardial infarction. *The American Journal of Cardiology*. 1991;68:7-16.
- [7] Wollert KC, Drexler H. Cell therapy for the treatment of coronary heart disease: a critical appraisal. *Nature reviews Cardiology*. 2010;7:204-15.
- [8] Chavakis E, Koyanagi M, Dimmeler S. Enhancing the outcome of cell therapy for cardiac repair: progress from bench to bedside and back. *Circulation*. 2010;121:325-35.
- [9] Hou J, Wang L, Jiang J, Zhou C, Guo T, Zheng S, et al. Cardiac Stem Cells and their Roles in Myocardial Infarction. *Stem cell reviews*. 2012.
- [10] Boyle AJ, Schulman SP, Hare JM, Oettgen P. Is stem cell therapy ready for patients? Stem Cell Therapy for Cardiac Repair. Ready for the Next Step. *Circulation*. 2006;114:339-52.
- [11] Min JY, Yang Y, Converso KL, Liu L, Huang Q, Morgan JP, et al. Transplantation of embryonic stem cells improves cardiac function in postinfarcted rats. *Journal of applied physiology* (Bethesda, Md : 1985). 2002;92:288-96.
- [12] Klug MG, Soonpaa MH, Koh GY, Field LJ. Genetically selected cardiomyocytes from differentiating embryonic stem cells form stable intracardiac grafts. *J Clin Invest*. 1996;98:216-24.
- [13] Wang D, Shen W, Zhang F, Chen M, Chen H, Cao K. Connexin43 promotes survival of mesenchymal stem cells in ischaemic heart. *Cell Biol Int*. 2010;34:415-23.

- [14] Angoulvant D, Ivanov F, Ferrera R, Matthews PG, Nataf S, Ovize M. Mesenchymal stem cell conditioned media attenuates in vitro and ex vivo myocardial reperfusion injury. *J Heart Lung Transplant*. 2011;30:95-102.
- [15] Herrmann JL, Abarbanell AM, Wang Y, Weil BR, Poynter JA, Manukyan MC, et al. Transforming Growth Factor- α Enhances Stem Cell-Mediated Postischemic Myocardial Protection. *Ann Thorac Surg*. 2011.
- [16] Williams AR, Trachtenberg B, Velazquez DL, McNiece I, Altman P, Rouy D, et al. Intramyocardial stem cell injection in patients with ischemic cardiomyopathy: functional recovery and reverse remodeling. *Circ Res*. 2011;108:792-6.
- [17] Leiker M, Suzuki G, Iyer VS, Canty JM, Jr., Lee T. Assessment of a nuclear affinity labeling method for tracking implanted mesenchymal stem cells. *Cell Transplant*. 2008;17:911-22.
- [18] Mirotsov M, Jayawardena TM, Schmeckpeper J, Gnecci M, Dzau VJ. Paracrine mechanisms of stem cell reparative and regenerative actions in the heart. *J Mol Cell Cardiol*. 2011;50:280-9.
- [19] Pijnappels DA, Gregoire S, Wu SM. The integrative aspects of cardiac physiology and their implications for cell-based therapy. *Annals of the New York Academy of Sciences*. 2010;1188:7-14.
- [20] Bers DM. Excitation – contraction coupling and cardiac contractile force. 2nd ed. Dordrecht, The Netherlands: : Kluwer Academic; 2003.
- [21] Michael G, Xiao L, Qi XY, Dobrev D, Nattel S. Remodelling of cardiac repolarization: how homeostatic responses can lead to arrhythmogenesis. *Cardiovascular research*. 2009;81:491-9.
- [22] Aiba T, Tomaselli GF. Electrical remodeling in the failing heart. *Current Opinion in Cardiology*. 2010;25:29-36.
- [23] Akar FG, Spragg DD, Tunin RS, Kass DA, Tomaselli GF. Mechanisms Underlying Conduction Slowing and Arrhythmogenesis in Nonischemic Dilated Cardiomyopathy. *Circulation Research*. 2004;95:717-25.
- [24] Tsuji Y, Zicha S, Qi XY, Kodama I, Nattel S. Potassium channel subunit remodeling in rabbits exposed to long-term bradycardia or tachycardia: discrete arrhythmogenic consequences related to differential delayed-rectifier changes. *Circulation*. 2006;113:345-55.

- [25] Kaab S, Dixon J, Duc J, Ashen D, Nabauer M, Beuckelmann DJ, et al. Molecular basis of transient outward potassium current downregulation in human heart failure: a decrease in Kv4.3 mRNA correlates with a reduction in current density. *Circulation*. 1998;98:1383-93.
- [26] Nabauer M, Beuckelmann DJ, Erdmann E. Characteristics of transient outward current in human ventricular myocytes from patients with terminal heart failure. *Circ Res*. 1993;73:386-94.
- [27] Beuckelmann DJ, Nabauer M, Erdmann E. Alterations of K⁺ currents in isolated human ventricular myocytes from patients with terminal heart failure. *Circ Res*. 1993;73:379-85.
- [28] January CT, Riddle JM. Early afterdepolarizations: mechanism of induction and block. A role for L-type Ca²⁺ current. *Circ Res*. 1989;64:977-90.
- [29] Sohl G, Willecke K. Gap junctions and the connexin protein family. *Cardiovascular research*. 2004;62:228-32.
- [30] Alexander DB, Goldberg GS. Transfer of biologically important molecules between cells through gap junction channels. *Current medicinal chemistry*. 2003;10:2045-58.
- [31] van Veen AA, van Rijen HV, Opthof T. Cardiac gap junction channels: modulation of expression and channel properties. *Cardiovascular research*. 2001;51:217-29.
- [32] Jalife J, Morley GE, Vaidya D. Connexins and impulse propagation in the mouse heart. *Journal of cardiovascular electrophysiology*. 1999;10:1649-63.
- [33] Gourdie RG, Severs NJ, Green CR, Rothery S, Germroth P, Thompson RP. The spatial distribution and relative abundance of gap-junctional connexin40 and connexin43 correlate to functional properties of components of the cardiac atrioventricular conduction system. *Journal of cell science*. 1993;105 (Pt 4):985-91.
- [34] Gros DB, Jongsma HJ. Connexins in mammalian heart function. *BioEssays : news and reviews in molecular, cellular and developmental biology*. 1996;18:719-30.
- [35] Saffitz JE, Kanter HL, Green KG, Tolley TK, Beyer EC. Tissue-specific determinants of anisotropic conduction velocity in canine atrial and ventricular myocardium. *Circ Res*. 1994;74:1065-70.
- [36] Rohr S. Role of gap junctions in the propagation of the cardiac action potential. *Cardiovascular research*. 2004;62:309-22.

- [37] Peters NS, Green CR, Poole-Wilson PA, Severs NJ. Reduced content of connexin43 gap junctions in ventricular myocardium from hypertrophied and ischemic human hearts. *Circulation*. 1993;88:864-75.
- [38] Fahrenbach JP, Mejia-Alvarez R, Banach K. The relevance of non-excitabile cells for cardiac pacemaker function. *J Physiol*. 2007;585:565-78.
- [39] Jacquemet V, Henriquez CS. Loading effect of fibroblast-myocyte coupling on resting potential, impulse propagation, and repolarization: insights from a microstructure model. *Am J Physiol Heart Circ Physiol*. 2008;294:H2040-52.
- [40] Williams AR, Hare JM. Mesenchymal stem cells: biology, pathophysiology, translational findings, and therapeutic implications for cardiac disease. *Circulation research*. 2011;109:923-40.
- [41] Gaudesius G, Miragoli M, Thomas SP, Rohr S. Coupling of cardiac electrical activity over extended distances by fibroblasts of cardiac origin. *Circ Res*. 2003;93:421.
- [42] Beeres SL, Atsma DE, van der Laarse A, Pijnappels DA, van Tuyn J, Fibbe WE, et al. Human adult bone marrow mesenchymal stem cells repair experimental conduction block in rat cardiomyocyte cultures. *J Am Coll Cardiol*. 2005;46:1943-52.
- [43] Wang D, Zhang F, Shen W, Chen M, Yang B, Zhang Y, et al. Mesenchymal stem cell injection ameliorates the inducibility of ventricular arrhythmias after myocardial infarction in rats. *Int J Cardiol*. 2011;152:314-20.
- [44] Askar SF, Ramkisoensing AA, Atsma DE, Schali J MJ, de Vries AA, Pijnappels DA. Engraftment Patterns of Human Adult Mesenchymal Stem Cells Expose Electrotonic and Paracrine Pro-Arrhythmic Mechanisms in Myocardial Cell Cultures. *Circulation Arrhythmia and electrophysiology*. 2013.
- [45] Valiunas V, Doronin S, Valiuniene L, Potapova I, Zuckerman J, Walcott B, et al. Human mesenchymal stem cells make cardiac connexins and form functional gap junctions. *J Physiol* 2004;555:617.
- [46] Quevedo HC, Hatzistergos KE, Oskoue BN, Feigenbaum GS, Rodriguez JE, Valdes D, et al. Allogeneic mesenchymal stem cells restore cardiac function in chronic ischemic cardiomyopathy via trilineage differentiating capacity. *Proc Natl Acad Sci U S A*. 2009;106:14022-7.

- [47] Chang MG, Tung L, Sekar RB, Chang CY, Cysyk J, Dong P, et al. Proarrhythmic potential of mesenchymal stem cell transplantation revealed in an in vitro coculture model. *Circulation*. 2006;113:1832-41.
- [48] Hahn JY, Cho HJ, Kang HJ, Kim TS, Kim MH, Chung JH, et al. Pre-treatment of mesenchymal stem cells with a combination of growth factors enhances gap junction formation, cytoprotective effect on cardiomyocytes, and therapeutic efficacy for myocardial infarction. *J Am Coll Cardiol*. 2008;51:933-43.
- [49] Mills WR, Mal N, Kiedrowski MJ, Unger R, Forudi F, Popovic ZB, et al. Stem cell therapy enhances electrical viability in myocardial infarction. *J Mol Cell Cardiol*. 2007;42:304-14.
- [50] Yokokawa M, Ohnishi S, Ishibashi-Ueda H, Obata H, Otani K, Miyahara Y, et al. Transplantation of mesenchymal stem cells improves atrioventricular conduction in a rat model of complete atrioventricular block. *Cell Transplant*. 2008;17:1145-55.
- [51] Kawano S, Otsu K, Kuruma A, Shoji S, Yanagida E, Muto Y, et al. ATP autocrine/paracrine signaling induces calcium oscillations and NFAT activation in human mesenchymal stem cells. *Cell Calcium*. 2006;39:313-24.
- [52] Psaltis PJ, Zannettino AC, Worthley SG, Gronthos S. Concise review: mesenchymal stromal cells: potential for cardiovascular repair. *Stem Cells*. 2008;26:2201-10.
- [53] Noiseux N, Gneocchi M, Lopez-Illasaca M, Zhang L, Solomon SD, Deb A, et al. Mesenchymal stem cells overexpressing Akt dramatically repair infarcted myocardium and improve cardiac function despite infrequent cellular fusion or differentiation. *Mol Ther*. 2006;14:840-50.
- [54] Gneocchi M, He H, Melo LG, Noiseux N, Morello F, de Boer RA, et al. Early beneficial effects of bone marrow-derived mesenchymal stem cells overexpressing Akt on cardiac metabolism after myocardial infarction. *Stem Cells*. 2009;27:971-9.
- [55] Cho J, Zhai P, Maejima Y, Sadoshima J. Myocardial Injection With GSK-3{beta}-Overexpressing Bone Marrow-Derived Mesenchymal Stem Cells Attenuates Cardiac Dysfunction After Myocardial Infarction. *Circ Res*. 2010.
- [56] Psaltis PJ, Paton S, See F, Arthur A, Martin S, Itescu S, et al. Enrichment for STRO-1 expression enhances the cardiovascular paracrine activity of human bone marrow-derived mesenchymal cell populations. *J Cell Physiol*. 2010;223:530-40.

- [57] Kinnaird T, Stabile E, Burnett MS, Shou M, Lee CW, Barr S, et al. Local delivery of marrow-derived stromal cells augments collateral perfusion through paracrine mechanisms. *Circulation*. 2004;109:1543-9.
- [58] Haider H, Jiang S, Idris NM, Ashraf M. IGF-1-overexpressing mesenchymal stem cells accelerate bone marrow stem cell mobilization via paracrine activation of SDF-1alpha/CXCR4 signaling to promote myocardial repair. *Circ Res*. 2008;103:1300-8.
- [59] Alfaro MP, Pagni M, Vincent A, Atkinson J, Hill MF, Cates J, et al. The Wnt modulator sFRP2 enhances mesenchymal stem cell engraftment, granulation tissue formation and myocardial repair. *Proc Natl Acad Sci U S A*. 2008;105:18366-71.
- [60] Mirotsoiu M, Zhang Z, Deb A, Zhang L, Gneccchi M, Noiseux N, et al. Secreted frizzled related protein 2 (Sfrp2) is the key Akt-mesenchymal stem cell-released paracrine factor mediating myocardial survival and repair. *Proc Natl Acad Sci U S A*. 2007;104:1643-8.
- [61] Desantiago J, Bare DJ, Semenov I, Minshall RD, Geenen DL, Wolska BM, et al. Excitation-contraction coupling in ventricular myocytes is enhanced by paracrine signaling from mesenchymal stem cells. *J Mol Cell Cardiol*. 2012;52:1249-56.
- [62] Markel TA, Wang Y, Herrmann JL, Crisostomo PR, Wang M, Novotny NM, et al. VEGF is critical for stem cell-mediated cardioprotection and a crucial paracrine factor for defining the age threshold in adult and neonatal stem cell function. *American journal of physiology Heart and circulatory physiology*. 2008;295:H2308-14.
- [63] Leroux L, Descamps B, Tojais NF, Seguy B, Oses P, Moreau C, et al. Hypoxia preconditioned mesenchymal stem cells improve vascular and skeletal muscle fiber regeneration after ischemia through a Wnt4-dependent pathway. *Molecular therapy : the journal of the American Society of Gene Therapy*. 2010;18:1545-52.
- [64] Pimentel RC, Yamada KA, Kleber AG, Saffitz JE. Autocrine regulation of myocyte Cx43 expression by VEGF. *Circ Res*. 2002;90:671-7.
- [65] Ai Z, Fischer A, Spray DC, Brown AM, Fishman GI. Wnt-1 regulation of connexin43 in cardiac myocytes. *J Clin Invest* 2000;105:161.
- [66] Boomsma RA, Swaminathan PD, Geenen DL. Intravenously injected mesenchymal stem cells home to viable myocardium after coronary occlusion and preserve systolic function without altering infarct size. *Int J Cardiol*. 2007;122:17-28.

- [67] Grajales L, Garcia J, Banach K, Geenen DL. Delayed enrichment of mesenchymal cells promotes cardiac lineage and calcium transient development. *J Mol Cell Cardiol.* 2010;48:735-45.
- [68] Halbach M, Egert U, Hescheler J, Banach K. Estimation of action potential changes from field potential recordings in multicellular mouse cardiac myocyte cultures. *Cell Physiol Biochem.* 2003;13:271-84.
- [69] Xiao L, Liu Q, Hu Z, Zhang W, Yu H, Wang P. A multi-scale electrode array (MSEA) to study excitation–contraction coupling of cardiomyocytes for high-throughput bioassays. *Sensors and Actuators B: Chemical.* 2011;152:107-14.
- [70] Claycomb WC, Lanson NA, Jr., Stallworth BS, Egeland DB, Delcarpio JB, Bahinski A, et al. HL-1 cells: a cardiac muscle cell line that contracts and retains phenotypic characteristics of the adult cardiomyocyte. *Proc Natl Acad Sci.* 1998;95:2979-84.
- [71] Fahrenbach JP, Ai X, Banach K. Decreased intercellular coupling improves the function of cardiac pacemakers derived from mouse embryonic stem cells. *J Mol Cell Cardiol.* 2008;45:642-9.
- [72] Prockop DJ, Sekiya I, Colter DC. Isolation and characterization of rapidly self-renewing stem cells from cultures of human marrow stromal cells. *Cytotherapy.* 2001;3:393-6.
- [73] Raaijmakers HG, Van Den Bosch G, Boezeman J, De Witte T, Raymakers RA. Single-cell image analysis to assess ABC-transporter-mediated efflux in highly purified hematopoietic progenitors. *Cytometry.* 2002;49:135-42.
- [74] Du WJ, Li JK, Wang QY, Hou JB, Yu B. Lithium chloride regulates connexin43 in skeletal myoblasts in vitro: possible involvement in Wnt/beta-catenin signaling. *Cell communication & adhesion.* 2008;15:261-71.
- [75] Cho M, Ryu M, Jeong Y, Chung YH, Kim DE, Cho HS, et al. Cardamonin suppresses melanogenesis by inhibition of Wnt/beta-catenin signaling. *Biochem Biophys Res Commun.* 2009;390:500-5.
- [76] Chen B, Dodge ME, Tang W, Lu J, Ma Z, Fan CW, et al. Small molecule-mediated disruption of Wnt-dependent signaling in tissue regeneration and cancer. *Nat Chem Biol.* 2009;5:100-7.
- [77] Mor M, Beharier O, Levy S, Kahn J, Dror S, Blumenthal D, et al. ZnT-1 enhances the activity and surface expression of T-type calcium channels through activation of Ras-ERK signaling. *American journal of physiology Cell physiology.* 2012;303:C192-203.

- [78] Shang YC, Wang SH, Xiong F, Zhao CP, Peng FN, Feng SW, et al. Wnt3a signaling promotes proliferation, myogenic differentiation, and migration of rat bone marrow mesenchymal stem cells. *Acta Pharmacol Sin*. 2007;28:1761-74.
- [79] Miragoli M, Gaudesius G, Rohr S. Electrotonic modulation of cardiac impulse conduction by myofibroblasts. *Circ Res*. 2006;98:801-10.
- [80] Mureli S, Gans CP, Bare DJ, Geenen DL, Kumar NM, Banach K. Mesenchymal stem cells improve cardiac conduction by upregulation of connexin 43 through paracrine signaling. *Am J Physiol Heart Circ Physiol*. 2013;304:H600-9.
- [81] Cho M, Ryu M, Jeong Y, Chung YH, Kim DE, Cho HS, et al. Cardamonin suppresses melanogenesis by inhibition of Wnt/beta-catenin signaling. *Biochem Biophys Res Commun*. 2009;390:500-5.
- [82] Haq S, Michael A, Andreucci M, Bhattacharya K, Dotto P, Walters B, et al. Stabilization of beta-catenin by a Wnt-independent mechanism regulates cardiomyocyte growth. *Proceedings of the National Academy of Sciences of the United States of America*. 2003;100:4610-5.
- [83] Archbold HC, Yang YX, Chen L, Cadigan KM. How do they do Wnt they do?: regulation of transcription by the Wnt/beta-catenin pathway. *Acta Physiol (Oxf)*. 2012;204:74-109.
- [84] von Marschall Z, Fisher LW. Secreted Frizzled-related protein-2 (sFRP2) augments canonical Wnt3a-induced signaling. *Biochem Biophys Res Commun*. 2010;400:299-304.
- [85] Okoye UC, Malbon CC, Wang HY. Wnt and Frizzled RNA expression in human mesenchymal and embryonic (H7) stem cells. *J Mol Signal*. 2008;3:16.
- [86] Chen B, Dodge ME, Tang W, Lu J, Ma Z, Fan CW, et al. Small molecule-mediated disruption of Wnt-dependent signaling in tissue regeneration and cancer. *Nat Chem Biol*. 2009;5:100-7.
- [87] Krejci P, Aklian A, Kaucka M, Sevcikova E, Prochazkova J, Masek JK, et al. Receptor Tyrosine Kinases Activate Canonical WNT/beta-Catenin Signaling via MAP Kinase/LRP6 Pathway and Direct beta-Catenin Phosphorylation. *PLoS One*. 2012;7:e35826.
- [88] Liu X, Ma B, Malik AB, Tang H, Yang T, Sun B, et al. Bidirectional regulation of neutrophil migration by mitogen-activated protein kinases. *Nat Immunol*. 2012;13:457-64.

- [89] Pijnappels DA, van Tuyn J, de Vries AA, Grauss RW, van der Laarse A, Ypey DL, et al. Resynchronization of separated rat cardiomyocyte fields with genetically modified human ventricular scar fibroblasts. *Circulation*. 2007;116:2018-28.
- [90] Ai X, Pogwizd SM. Connexin 43 downregulation and dephosphorylation in nonischemic heart failure is associated with enhanced colocalized protein phosphatase type 2A. *Circ Res*. 2005;96:54-63.
- [91] Aberg ND, Blomstrand F, Aberg MA, Bjorklund U, Carlsson B, Carlsson-Skwirut C, et al. Insulin-like growth factor-I increases astrocyte intercellular gap junctional communication and connexin43 expression in vitro. *J Neurosci Res*. 2003;74:12-22.
- [92] van der Heyden MA, Rook MB, Hermans MM, Rijksen G, Boonstra J, Defize LH, et al. Identification of connexin43 as a functional target for Wnt signalling. *J Cell Sci JID - 0052457*. 1998;111 (Pt 12):1741.
- [93] Salazar KD, Lankford SM, Brody AR. Mesenchymal stem cells produce Wnt isoforms and TGF-beta1 that mediate proliferation and procollagen expression by lung fibroblasts. *Am J Physiol Lung Cell Mol Physiol*. 2009;297:L1002-11.
- [94] Ling L, Nurcombe V, Cool SM. Wnt signaling controls the fate of mesenchymal stem cells. *Gene*. 2009;433:1-7.
- [95] Hannoush RN. Kinetics of Wnt-driven beta-catenin stabilization revealed by quantitative and temporal imaging. *PLoS One*. 2008;3:e3498.
- [96] Dunn CA, Su V, Lau AF, Lampe PD. Activation of Akt, not connexin 43 protein ubiquitination, regulates gap junction stability. *J Biol Chem*. 2012;287:2600-7.
- [97] Zeevi-Levin N, Barac YD, Reisner Y, Reiter I, Yaniv G, Meiry G, et al. Gap junctional remodeling by hypoxia in cultured neonatal rat ventricular myocytes. *Cardiovascular research*. 2005;66:64-73.
- [98] Zhang Z, Deb A, Zhang Z, Pachori A, He W, Guo J, et al. Secreted frizzled related protein 2 protects cells from apoptosis by blocking the effect of canonical Wnt3a. *J Mol Cell Cardiol*. 2009;46:370-7.
- [99] Dufourcq P, Descamps B, Tojais NF, Leroux L, Oses P, Daret D, et al. Secreted frizzled-related protein-1 enhances mesenchymal stem cell function in angiogenesis and contributes to neovessel maturation. *Stem Cells*. 2008;26:2991-3001.

- [100] Wu CY, Jia Z, Wang W, Ballou LM, Jiang YP, Chen B, et al. PI3Ks maintain the structural integrity of T-tubules in cardiac myocytes. *PLoS One*. 2011;6:e24404.
- [101] Louch WE, Sejersted OM, Swift F. There goes the neighborhood: pathological alterations in T-tubule morphology and consequences for cardiomyocyte Ca^{2+} handling. *Journal of biomedicine & biotechnology*. 2010;2010:503906.
- [102] Myklebust R, Saetersdal TS, Engedal H. The T-tubule system in the myocardia of the sand rat and mouse as demonstrated by horseradish peroxidase. *Cell and tissue research*. 1978;192:205-13.
- [103] Soeller C, Cannell MB. Examination of the transverse tubular system in living cardiac rat myocytes by 2-photon microscopy and digital image-processing techniques. *Circ Res*. 1999;84:266-75.
- [104] Haddock PS, Coetzee WA, Cho E, Porter L, Katoh H, Bers DM, et al. Subcellular $[\text{Ca}^{2+}]_i$ gradients during excitation-contraction coupling in newborn rabbit ventricular myocytes. *Circ Res*. 1999;85:415-27.
- [105] Heinzel FR, Bito V, Volders PG, Antoons G, Mubagwa K, Sipido KR. Spatial and temporal inhomogeneities during Ca^{2+} release from the sarcoplasmic reticulum in pig ventricular myocytes. *Circ Res*. 2002;91:1023-30.
- [106] He J, Conklin MW, Foell JD, Wolff MR, Haworth RA, Coronado R, et al. Reduction in density of transverse tubules and L-type Ca^{2+} channels in canine tachycardia-induced heart failure. *Cardiovascular research*. 2001;49:298-307.
- [107] Jayasinghe I, Crossman D, Soeller C, Cannell M. Comparison of the organization of T-tubules, sarcoplasmic reticulum and ryanodine receptors in rat and human ventricular myocardium. *Clinical and experimental pharmacology & physiology*. 2012;39:469-76.
- [108] Ayettey AS, Navaratnam V. The T-tubule system in the specialized and general myocardium of the rat. *Journal of anatomy*. 1978;127:125-40.
- [109] Kirk MM, Izu LT, Chen-Izu Y, McCulle SL, Wier WG, Balke CW, et al. Role of the transverse-axial tubule system in generating calcium sparks and calcium transients in rat atrial myocytes. *J Physiol*. 2003;547:441-51.
- [110] Dibb KM, Clarke JD, Horn MA, Richards MA, Graham HK, Eisner DA, et al. Characterization of an extensive transverse tubular network in sheep atrial myocytes and its depletion in heart failure. *Circulation Heart failure*. 2009;2:482-9.

- [111] Richards MA, Clarke JD, Saravanan P, Voigt N, Dobrev D, Eisner DA, et al. Transverse tubules are a common feature in large mammalian atrial myocytes including human. *Am J Physiol Heart Circ Physiol*. 2011;301:H1996-2005.
- [112] Brette F, Orchard C. T-tubule function in mammalian cardiac myocytes. *Circ Res*. 2003;92:1182-92.
- [113] Mitcheson JS, Hancox JC, Levi AJ. Action potentials, ion channel currents and transverse tubule density in adult rabbit ventricular myocytes maintained for 6 days in cell culture. *Pflugers Archiv : European journal of physiology*. 1996;431:814-27.
- [114] Lyon AR, MacLeod KT, Zhang Y, Garcia E, Kanda GK, Lab MJ, et al. Loss of T-tubules and other changes to surface topography in ventricular myocytes from failing human and rat heart. *Proc Natl Acad Sci U S A*. 2009;106:6854-9.
- [115] Ibrahim M, Gorelik J, Yacoub MH, Terracciano CM. The structure and function of cardiac t-tubules in health and disease. *Proceedings Biological sciences / The Royal Society*. 2011;278:2714-23.
- [116] Lee E, Marcucci M, Daniell L, Pypaert M, Weisz OA, Ochoa GC, et al. Amphiphysin 2 (Bin1) and T-tubule biogenesis in muscle. *Science (New York, NY)*. 2002;297:1193-6.
- [117] Muller AJ, Baker JF, DuHadaway JB, Ge K, Farmer G, Donover PS, et al. Targeted disruption of the murine Bin1/Amphiphysin II gene does not disable endocytosis but results in embryonic cardiomyopathy with aberrant myofibril formation. *Molecular and cellular biology*. 2003;23:4295-306.
- [118] Hong TT, Smyth JW, Gao D, Chu KY, Vogan JM, Fong TS, et al. BIN1 localizes the L-type calcium channel to cardiac T-tubules. *PLoS biology*. 2010;8:e1000312.
- [119] Takeshima H, Komazaki S, Nishi M, Iino M, Kangawa K. Junctophilins: a novel family of junctional membrane complex proteins. *Molecular cell*. 2000;6:11-22.
- [120] Wei S, Guo A, Chen B, Kutschke W, Xie YP, Zimmerman K, et al. T-tubule remodeling during transition from hypertrophy to heart failure. *Circ Res*. 2010;107:520-31.
- [121] Balijepalli RC, Lokuta AJ, Maertz NA, Buck JM, Haworth RA, Valdivia HH, et al. Depletion of T-tubules and specific subcellular changes in sarcolemmal proteins in tachycardia-induced heart failure. *Cardiovascular research*. 2003;59:67-77.

- [122] Heinzel FR, Bito V, Biesmans L, Wu M, Detre E, von Wegner F, et al. Remodeling of T-tubules and reduced synchrony of Ca²⁺ release in myocytes from chronically ischemic myocardium. *Circ Res*. 2008;102:338-46.
- [123] Gomez AM, Valdivia HH, Cheng H, Lederer MR, Santana LF, Cannell MB, et al. Defective excitation-contraction coupling in experimental cardiac hypertrophy and heart failure. *Science* (New York, NY). 1997;276:800-6.
- [124] Louch WE, Bito V, Heinzel FR, Macianskiene R, Vanhaecke J, Flameng W, et al. Reduced synchrony of Ca²⁺ release with loss of T-tubules-a comparison to Ca²⁺ release in human failing cardiomyocytes. *Cardiovascular research*. 2004;62:63-73.
- [125] Murdoch CE, Zhang M, Cave AC, Shah AM. NADPH oxidase-dependent redox signalling in cardiac hypertrophy, remodelling and failure. *Cardiovascular research*. 2006;71:208-15.
- [126] McMurray J, Chopra M, Abdullah I, Smith WE, Dargie HJ. Evidence of oxidative stress in chronic heart failure in humans. *European heart journal*. 1993;14:1493-8.
- [127] Cheng TH, Cheng PY, Shih NL, Chen IB, Wang DL, Chen JJ. Involvement of reactive oxygen species in angiotensin II-induced endothelin-1 gene expression in rat cardiac fibroblasts. *J Am Coll Cardiol*. 2003;42:1845-54.
- [128] Spinale FG. Bioactive peptide signaling within the myocardial interstitium and the matrix metalloproteinases. *Circ Res*. 2002;91:1082-4.
- [129] Siwik DA, Pagano PJ, Colucci WS. Oxidative stress regulates collagen synthesis and matrix metalloproteinase activity in cardiac fibroblasts. *American journal of physiology Cell physiology*. 2001;280:C53-60.
- [130] Kawakami M, Okabe E. Superoxide anion radical-triggered Ca²⁺ release from cardiac sarcoplasmic reticulum through ryanodine receptor Ca²⁺ channel. *Molecular pharmacology*. 1998;53:497-503.
- [131] Fearon IM, Palmer AC, Balmforth AJ, Ball SG, Varadi G, Peers C. Modulation of recombinant human cardiac L-type Ca²⁺ channel alpha1C subunits by redox agents and hypoxia. *J Physiol*. 1999;514 (Pt 3):629-37.
- [132] Giordano FJ. Oxygen, oxidative stress, hypoxia, and heart failure. *J Clin Invest*. 2005;115:500-8.

- [133] Li JM, Gall NP, Grieve DJ, Chen M, Shah AM. Activation of NADPH oxidase during progression of cardiac hypertrophy to failure. *Hypertension*. 2002;40:477-84.
- [134] Heymes C, Bendall JK, Ratajczak P, Cave AC, Samuel JL, Hasenfuss G, et al. Increased myocardial NADPH oxidase activity in human heart failure. *J Am Coll Cardiol*. 2003;41:2164-71.
- [135] Bendall JK, Cave AC, Heymes C, Gall N, Shah AM. Pivotal role of a gp91(phox)-containing NADPH oxidase in angiotensin II-induced cardiac hypertrophy in mice. *Circulation*. 2002;105:293-6.
- [136] Landmesser U, Dikalov S, Price SR, McCann L, Fukai T, Holland SM, et al. Oxidation of tetrahydrobiopterin leads to uncoupling of endothelial cell nitric oxide synthase in hypertension. *J Clin Invest*. 2003;111:1201-9.
- [137] McNally JS, Davis ME, Giddens DP, Saha A, Hwang J, Dikalov S, et al. Role of xanthine oxidoreductase and NAD(P)H oxidase in endothelial superoxide production in response to oscillatory shear stress. *Am J Physiol Heart Circ Physiol*. 2003;285:H2290-7.
- [138] Jaime DeSantiago DB, Yunbo Ke, R. John Solaro, Kathrin Banach. p21-Activated Kinase (Pak1) is a Negative Regulator of ROS Generation in Ventricular Myocytes. Biophysical Society Meeting. Philadelphia, Pennsylvania, USA: Abstracts. *Biophysical Journal*, Supplement; 2013. p. 614a.
- [139] Tian Q, Pahlavan S, Oleinikow K, Jung J, Ruppenthal S, Scholz A, et al. Functional and morphological preservation of adult ventricular myocytes in culture by sub-micromolar cytochalasin D supplement. *J Mol Cell Cardiol*. 2012;52:113-24.
- [140] Leach RN, Desai JC, Orchard CH. Effect of cytoskeleton disruptors on L-type Ca channel distribution in rat ventricular myocytes. *Cell Calcium*. 2005;38:515-26.
- [141] Domeier TL, Zima AV, Maxwell JT, Huke S, Mignery GA, Blatter LA. IP3 receptor-dependent Ca²⁺ release modulates excitation-contraction coupling in rabbit ventricular myocytes. *Am J Physiol Heart Circ Physiol*. 2008;294:H596-604.
- [142] Bassani RA, Bassani JW, Bers DM. Mitochondrial and sarcolemmal Ca²⁺ transport reduce [Ca²⁺]_i during caffeine contractures in rabbit cardiac myocytes. *J Physiol*. 1992;453:591-608.
- [143] Pavlovic D, McLatchie LM, Shattock MJ. The rate of loss of T-tubules in cultured adult ventricular myocytes is species dependent. *Experimental physiology*. 2010;95:518-27.

- [144] Ellingsen O, Davidoff AJ, Prasad SK, Berger HJ, Springhorn JP, Marsh JD, et al. Adult rat ventricular myocytes cultured in defined medium: phenotype and electromechanical function. *The American journal of physiology*. 1993;265:H747-54.
- [145] Zeng Q, Zhou Q, Yao F, O'Rourke ST, Sun C. Endothelin-1 regulates cardiac L-type calcium channels via NAD(P)H oxidase-derived superoxide. *The Journal of pharmacology and experimental therapeutics*. 2008;326:732-8.
- [146] Tsai CT, Tseng CD, Hwang JJ, Wu CK, Yu CC, Wang YC, et al. Tachycardia of atrial myocytes induces collagen expression in atrial fibroblasts through transforming growth factor beta1. *Cardiovascular research*. 2011;89:805-15.
- [147] Liu M, Gu L, Sulkin MS, Liu H, Jeong EM, Greener I, et al. Mitochondrial dysfunction causing cardiac sodium channel downregulation in cardiomyopathy. *J Mol Cell Cardiol*. 2013;54:25-34.
- [148] Hammer K, Ruppenthal S, Viero C, Scholz A, Edelmann L, Kaestner L, et al. Remodelling of Ca²⁺ handling organelles in adult rat ventricular myocytes during long term culture. *J Mol Cell Cardiol*. 2010;49:427-37.
- [149] Tomori K, Ohta Y, Nishizawa T, Tamaki H, Takekura H. Low-intensity electrical stimulation ameliorates disruption of transverse tubules and neuromuscular junctional architecture in denervated rat skeletal muscle fibers. *Journal of muscle research and cell motility*. 2010;31:195-205.
- [150] Gonzales RCW, Richard E. Thresholding In Digital Image Processing: Pearson Education 2002.
- [151] Tukey JWC, JW. An algorithm for the machine calculation of complex Fourier series. *Math Comput*. 1965;19:297-301.
- [152] Takimoto E, Kass DA. Role of oxidative stress in cardiac hypertrophy and remodeling. *Hypertension*. 2007;49:241-8.
- [153] Grieve DJ, Byrne JA, Siva A, Layland J, Johar S, Cave AC, et al. Involvement of the nicotinamide adenosine dinucleotide phosphate oxidase isoform Nox2 in cardiac contractile dysfunction occurring in response to pressure overload. *J Am Coll Cardiol*. 2006;47:817-26.
- [154] Hsu HH, Hoffmann S, Endlich N, Velic A, Schwab A, Weide T, et al. Mechanisms of angiotensin II signaling on cytoskeleton of podocytes. *Journal of molecular medicine (Berlin, Germany)*. 2008;86:1379-94.

[155] Peng T, Lu X, Feng Q. Pivotal role of gp91phox-containing NADH oxidase in lipopolysaccharide-induced tumor necrosis factor- α expression and myocardial depression. *Circulation*. 2005;111:1637-44.

VITA

NAME: Shwetha Mureli

EDUCATION: B.Tech., Bioinformatics, SASTRA University, India, 2010

PROFESSIONAL
MEMBERSHIP: The American Physiological Society

PUBLICATIONS: Mureli, S, Gans, C.P., Bare, D.J., Geenen, D.L., Kumar, N.M., Banach, K.: Mesenchymal stem cells improve cardiac conduction by upregulation of connexin 43 through paracrine signaling. Am. J. Physiol. Heart Circ. Physiol. 304:H600-9, 2013

Pereira, M.J., Ouyang, B., Sundback, C.A., Lang, N., Friehs, I., Mureli, S., Pomerantseva, I., McFadden, J., Mochel, M.C., Mwizerwa, O., Del Nido, P., Sarkar, D., Masiakos, P.T., Langer, R., Ferreira, L.S., Karp, J.M.: A highly tunable biocompatible and multifunctional biodegradable elastomer. Advanced Materials 25: 1209-15, 2013

BOOK CHAPTERS: Cho, W.K., Pereira, M.N., Lang, N., Lee, K., Mureli, S., Zumbeuhl, A., Sundback, C.A., Masiakos, P.T., Carter, D.J., Borenstein, J., Ferreira, L., Langer, R., Karp, J.M.: Gecko-inspired tape-based adhesives: Engineering Biomaterials. In: Regenerative Medicine: Novel Technologies for Clinical Applications, pp. 195-225, Springer Publisher, 2011

Department of Bioengineering (MC 063)
Science and Engineering Offices
851 South Morgan Street, Room 218
Chicago, Illinois 60607-7052

Feb 18 2013

Dear Dr. Christopher Gans,

I am writing to request permission to use the following material from our publication (Mureli S et al, Mesenchymal Stem Cells Improve Cardiac Conduction by Up-regulation of Connexin 43 Through Paracrine Signaling, *Am J Physiol Heart Circ Physiol* (2012) Dec 15 [Epub ahead of print]) in my Masters thesis. This material will appear as originally published. Unless you request otherwise, I will use the conventional style of the Graduate College of the University of Illinois at Chicago as acknowledgment.

Material to be used:

a) Methods:

- (i) Conditioned Medium (ConM) preparation
- (ii) Co-culture and dye diffusion assay
- (iii) Quantitative reverse transcriptase polymerase chain reaction (RT-PCR)

b) Results & Figures:

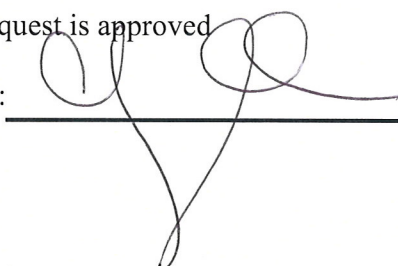
- (i) MSCs modulate the spontaneous activity of HL-1 cells [Figure 1(A)].
- (ii) HL-1 cells and MSCs establish intercellular coupling via gap junctions [Figure 1(B,C,D), 2A].
- (iii) MSC-conditioned medium increases connexin 43 expression in cardiomyocytes [Figure (3A, B)].

A copy of this letter is included for your records. Thank you for your kind consideration of this request.

Sincerely,
Shwetha Mureli
840 South Wood St
Chicago Illinois 60612
Ph: 336-508-6390

The above request is approved

Approved by:

 CHRISTOPHER GANS Date: 2/19/13

Department of Bioengineering (MC 063)
Science and Engineering Offices
851 South Morgan Street, Room 218
Chicago, Illinois 60607-7052

Feb 21 2013

Dear Dr. Dan J. Bare,

I am writing to request permission to use the following material from our publication (Mureli S et al, Mesenchymal Stem Cells Improve Cardiac Conduction by Upregulation of Connexin 43 Through Paracrine Signaling; *Am J Physiol Heart Circ Physiol* 304: H600-H609, 2013) in my Masters thesis. This material will appear as originally published. Unless you request otherwise, I will use the conventional style of the Graduate College of the University of Illinois at Chicago as acknowledgment.

Material to be used:

a) Methods:

- (i) Conditioned Tyrode (ConT) preparation
- (ii) HL-1 cell treatment, sample preparation, SDS-PAGE and western blotting procedures

b) Results & Figures:

- (i) MSC-conditioned medium and ConT increase Cx43 expression in cardiomyocytes [Fig. (3C, D)].
- (ii) β -Catenin inhibition prevents the ConT-mediated increase in Cx43 protein [Fig. (4A)].
- (iii) Lithium inhibition of GSK-3 β mimics the effect of ConT on Cx43 protein expression [Fig. (5A)].
- (iv) ConM changes in Cx43 does not depend on PI3-kinase /Akt signaling but elevates p-ERK1/2 [Fig. (6A,B)].
- (v) ConT-mediated changes depend upon activation of p-LRP6 and p-ERK 1/2 signal transduction [Fig. (7A,C)].

A copy of this letter is included for your records. Thank you for your kind consideration of this request.

Sincerely,

Shwetha Mureli
840 South Wood St
Chicago Illinois 60612
Ph: 336-508-6390

The above request is approved.

Approved by: _____

Date: _____

DAN J. BARE, Ph.D.

**OXFORD UNIVERSITY PRESS LICENSE
TERMS AND CONDITIONS**

Mar 04, 2013

This is a License Agreement between Shwetha Mureli ("You") and Oxford University Press ("Oxford University Press") provided by Copyright Clearance Center ("CCC"). The license consists of your order details, the terms and conditions provided by Oxford University Press, and the payment terms and conditions.

All payments must be made in full to CCC. For payment instructions, please see information listed at the bottom of this form.

License Number	3102041319979
License date	Mar 04, 2013
Licensed content publisher	Oxford University Press
Licensed content publication	Cardiovascular Research
Licensed content title	Remodelling of cardiac repolarization: how homeostatic responses can lead to arrhythmogenesis:
Licensed content author	Georghia Michael, Ling Xiao, Xiao-Yan Qi, Dobromir Dobrev, Stanley Nattel
Licensed content date	09/30/2008
Type of Use	Thesis/Dissertation
Institution name	
Title of your work	Pathophysiological Cardiac Remodeling And The Potential Of Cellular And Molecular Therapy
Publisher of your work	n/a
Expected publication date	Mar 2013
Permissions cost	0.00 USD
Value added tax	0.00 USD
Total	0.00 USD
Total	0.00 USD

Terms and Conditions**STANDARD TERMS AND CONDITIONS FOR REPRODUCTION OF
MATERIAL FROM AN OXFORD UNIVERSITY PRESS JOURNAL**

1. Use of the material is restricted to the type of use specified in your order details.
2. This permission covers the use of the material in the English language in the following territory: world. If you have requested additional permission to translate this material, the terms and conditions of this reuse will be set out in clause 12.

3. This permission is limited to the particular use authorized in (1) above and does not allow you to sanction its use elsewhere in any other format other than specified above, nor does it apply to quotations, images, artistic works etc that have been reproduced from other sources which may be part of the material to be used.

4. No alteration, omission or addition is made to the material without our written consent. Permission must be re-cleared with Oxford University Press if/when you decide to reprint.

5. The following credit line appears wherever the material is used: author, title, journal, year, volume, issue number, pagination, by permission of Oxford University Press or the sponsoring society if the journal is a society journal. Where a journal is being published on behalf of a learned society, the details of that society must be included in the credit line.

6. For the reproduction of a full article from an Oxford University Press journal for whatever purpose, the corresponding author of the material concerned should be informed of the proposed use. Contact details for the corresponding authors of all Oxford University Press journal contact can be found alongside either the abstract or full text of the article concerned, accessible from www.oxfordjournals.org Should there be a problem clearing these rights, please contact journals.permissions@oxfordjournals.org

7. If the credit line or acknowledgement in our publication indicates that any of the figures, images or photos was reproduced, drawn or modified from an earlier source it will be necessary for you to clear this permission with the original publisher as well. If this permission has not been obtained, please note that this material cannot be included in your publication/photocopies.

8. While you may exercise the rights licensed immediately upon issuance of the license at the end of the licensing process for the transaction, provided that you have disclosed complete and accurate details of your proposed use, no license is finally effective unless and until full payment is received from you (either by Oxford University Press or by Copyright Clearance Center (CCC)) as provided in CCC's Billing and Payment terms and conditions. If full payment is not received on a timely basis, then any license preliminarily granted shall be deemed automatically revoked and shall be void as if never granted. Further, in the event that you breach any of these terms and conditions or any of CCC's Billing and Payment terms and conditions, the license is automatically revoked and shall be void as if never granted. Use of materials as described in a revoked license, as well as any use of the materials beyond the scope of an unrevoked license, may constitute copyright infringement and Oxford University Press reserves the right to take any and all action to protect its copyright in the materials.

9. This license is personal to you and may not be sublicensed, assigned or transferred by you to any other person without Oxford University Press's written permission.

10. Oxford University Press reserves all rights not specifically granted in the combination of (i) the license details provided by you and accepted in the course of this licensing transaction, (ii) these terms and conditions and (iii) CCC's Billing and Payment terms and conditions.

11. You hereby indemnify and agree to hold harmless Oxford University Press and CCC, and their respective officers, directors, employs and agents, from and against any and all claims arising out of your use of the licensed material other than as specifically authorized pursuant to this license.

12. Other Terms and Conditions:

**OXFORD UNIVERSITY PRESS LICENSE
TERMS AND CONDITIONS**

Feb 26, 2013

This is a License Agreement between Shwetha Mureli ("You") and Oxford University Press ("Oxford University Press") provided by Copyright Clearance Center ("CCC"). The license consists of your order details, the terms and conditions provided by Oxford University Press, and the payment terms and conditions.

All payments must be made in full to CCC. For payment instructions, please see information listed at the bottom of this form.

License Number	3096431238956
License date	Feb 26, 2013
Licensed content publisher	Oxford University Press
Licensed content publication	Cardiovascular Research
Licensed content title	Gap junctions and the connexin protein family:
Licensed content author	Goran Söhl, Klaus Willecke
Licensed content date	05/01/2004
Type of Use	Thesis/Dissertation
Institution name	
Title of your work	Pathophysiological Cardiac Remodeling And The Potential Of Cellular And Molecular Therapy
Publisher of your work	n/a
Expected publication date	Mar 2013
Permissions cost	0.00 USD
Value added tax	0.00 USD
Total	0.00 USD
Total	0.00 USD

Terms and Conditions**STANDARD TERMS AND CONDITIONS FOR REPRODUCTION OF
MATERIAL FROM AN OXFORD UNIVERSITY PRESS JOURNAL**

1. Use of the material is restricted to the type of use specified in your order details.
2. This permission covers the use of the material in the English language in the following territory: world. If you have requested additional permission to translate this material, the terms and conditions of this reuse will be set out in clause 12.
3. This permission is limited to the particular use authorized in (1) above and does not allow you to sanction its use elsewhere in any other format other than specified above, nor does it

apply to quotations, images, artistic works etc that have been reproduced from other sources which may be part of the material to be used.

4. No alteration, omission or addition is made to the material without our written consent. Permission must be re-cleared with Oxford University Press if/when you decide to reprint.

5. The following credit line appears wherever the material is used: author, title, journal, year, volume, issue number, pagination, by permission of Oxford University Press or the sponsoring society if the journal is a society journal. Where a journal is being published on behalf of a learned society, the details of that society must be included in the credit line.

6. For the reproduction of a full article from an Oxford University Press journal for whatever purpose, the corresponding author of the material concerned should be informed of the proposed use. Contact details for the corresponding authors of all Oxford University Press journal contact can be found alongside either the abstract or full text of the article concerned, accessible from www.oxfordjournals.org Should there be a problem clearing these rights, please contact journals.permissions@oxfordjournals.org

7. If the credit line or acknowledgement in our publication indicates that any of the figures, images or photos was reproduced, drawn or modified from an earlier source it will be necessary for you to clear this permission with the original publisher as well. If this permission has not been obtained, please note that this material cannot be included in your publication/photocopies.

8. While you may exercise the rights licensed immediately upon issuance of the license at the end of the licensing process for the transaction, provided that you have disclosed complete and accurate details of your proposed use, no license is finally effective unless and until full payment is received from you (either by Oxford University Press or by Copyright Clearance Center (CCC)) as provided in CCC's Billing and Payment terms and conditions. If full payment is not received on a timely basis, then any license preliminarily granted shall be deemed automatically revoked and shall be void as if never granted. Further, in the event that you breach any of these terms and conditions or any of CCC's Billing and Payment terms and conditions, the license is automatically revoked and shall be void as if never granted. Use of materials as described in a revoked license, as well as any use of the materials beyond the scope of an unrevoked license, may constitute copyright infringement and Oxford University Press reserves the right to take any and all action to protect its copyright in the materials.

9. This license is personal to you and may not be sublicensed, assigned or transferred by you to any other person without Oxford University Press's written permission.

10. Oxford University Press reserves all rights not specifically granted in the combination of (i) the license details provided by you and accepted in the course of this licensing transaction, (ii) these terms and conditions and (iii) CCC's Billing and Payment terms and conditions.

11. You hereby indemnify and agree to hold harmless Oxford University Press and CCC, and their respective officers, directors, employs and agents, from and against any and all claims arising out of your use of the licensed material other than as specifically authorized pursuant to this license.

12. Other Terms and Conditions:

v1.4

**ELSEVIER LICENSE
TERMS AND CONDITIONS**

Mar 19, 2013

This is a License Agreement between Shwetha Mureli ("You") and Elsevier ("Elsevier") provided by Copyright Clearance Center ("CCC"). The license consists of your order details, the terms and conditions provided by Elsevier, and the payment terms and conditions.

All payments must be made in full to CCC. For payment instructions, please see information listed at the bottom of this form.

Supplier	Elsevier Limited The Boulevard, Langford Lane Kidlington, Oxford, OX5 1GB, UK
Registered Company Number	1982084
Customer name	Shwetha Mureli
Customer address	2306 W Taylor St Chicago, IL 60612
License number	3112601343282
License date	Mar 19, 2013
Licensed content publisher	Elsevier
Licensed content publication	Sensors and Actuators B: Chemical
Licensed content title	A multi-scale electrode array (MSEA) to study excitation-contraction coupling of cardiomyocytes for high-throughput bioassays
Licensed content author	Lidan Xiao, Qingjun Liu, Zhaoying Hu, Wei Zhang, Hui Yu, Ping Wang
Licensed content date	20 February 2011
Licensed content volume number	152
Licensed content issue number	1
Number of pages	8
Start Page	107
End Page	114
Type of Use	reuse in a thesis/dissertation
Intended publisher of new work	other
Portion	figures/tables/illustrations
Number of figures/tables/illustrations	1
Format	both print and electronic

Are you the author of this Elsevier article? No

Will you be translating? No

Order reference number

Title of your thesis/dissertation Pathophysiological Cardiac Remodeling And The Potential Of Cellular And Molecular Therapy

Expected completion date Mar 2013

Estimated size (number of pages) 50

Elsevier VAT number GB 494 6272 12

Permissions price 0.00 USD

VAT/Local Sales Tax 0.0 USD / 0.0 GBP

Total 0.00 USD

Terms and Conditions

INTRODUCTION

1. The publisher for this copyrighted material is Elsevier. By clicking "accept" in connection with completing this licensing transaction, you agree that the following terms and conditions apply to this transaction (along with the Billing and Payment terms and conditions established by Copyright Clearance Center, Inc. ("CCC"), at the time that you opened your Rightslink account and that are available at any time at <http://myaccount.copyright.com>).

GENERAL TERMS

2. Elsevier hereby grants you permission to reproduce the aforementioned material subject to the terms and conditions indicated.

3. Acknowledgement: If any part of the material to be used (for example, figures) has appeared in our publication with credit or acknowledgement to another source, permission must also be sought from that source. If such permission is not obtained then that material may not be included in your publication/copies. Suitable acknowledgement to the source must be made, either as a footnote or in a reference list at the end of your publication, as follows:

“Reprinted from Publication title, Vol /edition number, Author(s), Title of article / title of chapter, Pages No., Copyright (Year), with permission from Elsevier [OR APPLICABLE SOCIETY COPYRIGHT OWNER].” Also Lancet special credit - “Reprinted from The Lancet, Vol. number, Author(s), Title of article, Pages No., Copyright (Year), with permission from Elsevier.”

4. Reproduction of this material is confined to the purpose and/or media for which permission is hereby given.

5. Altering/Modifying Material: Not Permitted. However figures and illustrations may be altered/adapted minimally to serve your work. Any other abbreviations, additions, deletions and/or any other alterations shall be made only with prior written authorization of Elsevier Ltd. (Please contact Elsevier at permissions@elsevier.com)

6. If the permission fee for the requested use of our material is waived in this instance, please

be advised that your future requests for Elsevier materials may attract a fee.

7. **Reservation of Rights:** Publisher reserves all rights not specifically granted in the combination of (i) the license details provided by you and accepted in the course of this licensing transaction, (ii) these terms and conditions and (iii) CCC's Billing and Payment terms and conditions.

8. **License Contingent Upon Payment:** While you may exercise the rights licensed immediately upon issuance of the license at the end of the licensing process for the transaction, provided that you have disclosed complete and accurate details of your proposed use, no license is finally effective unless and until full payment is received from you (either by publisher or by CCC) as provided in CCC's Billing and Payment terms and conditions. If full payment is not received on a timely basis, then any license preliminarily granted shall be deemed automatically revoked and shall be void as if never granted. Further, in the event that you breach any of these terms and conditions or any of CCC's Billing and Payment terms and conditions, the license is automatically revoked and shall be void as if never granted. Use of materials as described in a revoked license, as well as any use of the materials beyond the scope of an unrevoked license, may constitute copyright infringement and publisher reserves the right to take any and all action to protect its copyright in the materials.

9. **Warranties:** Publisher makes no representations or warranties with respect to the licensed material.

10. **Indemnity:** You hereby indemnify and agree to hold harmless publisher and CCC, and their respective officers, directors, employees and agents, from and against any and all claims arising out of your use of the licensed material other than as specifically authorized pursuant to this license.

11. **No Transfer of License:** This license is personal to you and may not be sublicensed, assigned, or transferred by you to any other person without publisher's written permission.

12. **No Amendment Except in Writing:** This license may not be amended except in a writing signed by both parties (or, in the case of publisher, by CCC on publisher's behalf).

13. **Objection to Contrary Terms:** Publisher hereby objects to any terms contained in any purchase order, acknowledgment, check endorsement or other writing prepared by you, which terms are inconsistent with these terms and conditions or CCC's Billing and Payment terms and conditions. These terms and conditions, together with CCC's Billing and Payment terms and conditions (which are incorporated herein), comprise the entire agreement between you and publisher (and CCC) concerning this licensing transaction. In the event of any conflict between your obligations established by these terms and conditions and those established by CCC's Billing and Payment terms and conditions, these terms and conditions shall control.

14. **Revocation:** Elsevier or Copyright Clearance Center may deny the permissions described in this License at their sole discretion, for any reason or no reason, with a full refund payable to you. Notice of such denial will be made using the contact information provided by you. Failure to receive such notice will not alter or invalidate the denial. In no event will Elsevier or Copyright Clearance Center be responsible or liable for any costs, expenses or damage incurred by you as a result of a denial of your permission request, other than a refund of the amount(s) paid by you to Elsevier and/or Copyright Clearance Center for denied permissions.

LIMITED LICENSE